Taylor & Francis
Taylor & Francis Group

Orthogonal Polynomials with Respect to Self-Similar Measures

Steven M. Heilman, Philip Owrutsky, and Robert S. Strichartz

CONTENTS

We study experimentally systems of orthogonal polynomials with respect to self-similar measures. When the support of the measure is a Cantor set, we observe some interesting properties of the polynomials, both on the Cantor set and in the gaps of the Cantor set. We introduce an effective method to visualize the graph of a function on a Cantor set. We suggest a new perspective, based on the theory of dynamical systems, for studying families $P_n(x)$ of orthogonal functions as functions of n for fixed values of x.

1. INTRODUCTION

The classical theory of orthogonal polynomials [Gautschi 04, Szegő 75] allows one to start the Gram–Schmidt process with virtually any measure. In the families of polynomials that are usually studied, the measure is either absolutely continuous or discrete, but the general theory allows one to use a singular continuous measure. In recent years there has been an interest in the case of fractal measures. See, for example, [Barnsley et al. 83a, Barnsley et al. 83b, Barnsley et al. 85, Bessis and Moussa 83, Mantica 96, Mantica 97a, Mantica 97b, Mantica 98a, Mantica 98b, Mantica 00]. In particular, G. Mantica has developed algorithms to efficiently compute the coefficients of the 3-term recurrence relation, and hence the polynomials, in the case of a self-similar measure [Mantica 96, Mantica 00]. In this work we use these algorithms as a tool to study the polynomials experimentally, looking for interesting patterns and conjectures. We view this as part of a general program to explore portions of classical analysis related to fractal measures.

Let μ be a measure on the line, and for simplicity assume that μ is a probability measure supported on the unit interval. The related system $\{P_n(x)\}$ of orthogonal polynomials is characterized as follows:

1. $P_n(x)$ is a polynomial of degree n with a nonnegative coefficient of x^n.

2. Orthonormality:

$$\int P_n(x)P_m(x)d\mu(x) = \delta_{n,m}.$$

The general theory implies that there is a 3-term recurrence relation

$$xP_n(x) = r_{n+1}P_{n+1}(x) + A_nP_n(x) + r_nP_{n-1}, \quad (1\text{--}1)$$

where $r_n, A_n > 0$, $n \in \mathbb{Z}^+$ are determined by the measure μ and $P_{-1} = 0$, $P_0 = 1$. The coefficients r_n, A_n are also called the entries of the *Jacobi matrix*, an infinite symmetric tridiagonal matrix J such that $J_{i,i} = A_i$ and $J_{i,i+1} = J_{i+1,i} = r_{i+1}$ for $i \in \mathbb{Z}^{\geq 0}$. Note that (1–1) allows us to find the polynomials recursively:

$$P_{n+1}(x) = \frac{1}{r_{n+1}}((x - A_n)P_n(x)) - \frac{r_n}{r_{n+1}}P_{n-1}(x).$$

$$(1\text{--}2)$$

We should point out that while in principle (1–2) allows computation of the coefficients of P_n, this computation could be unstable. In the case that A_n is constant (as we shall see below when our measure is supported on a Cantor set), it is often easier to compute the coefficients of P_n as a polynomial in $(x - A_n)$. When the A_n vary, we alternatively use (1–2) to compute the values $P_n(x)$ for specific x-values.

A measure μ on the line is said to be self-similar if there exist an iterated function system (IFS) of contractive similarities $\{F_i\}_{i=1}^N$ and a set of probability weights $\{p_i\}_{i=1}^N$ such that

$$\mu(A) = \sum_{i=1}^N p_i\mu(F_i^{-1}A)$$

for any measurable set A, or equivalently,

$$\int f\,d\mu = \sum_{i=1}^N p_i \int f \circ F_i\,d\mu$$

for any continuous function f. In this paper we restrict our attention to the family of IFSs with $N = 2$ and such that

$$F_1(x) = \frac{1}{R}x, \quad F_2(x) = \frac{1}{R}(x - 1) + 1,$$

where $R \geq 2$ is a parameter. When $R = 2$ and $p_1 = P_2 = \frac{1}{2}$, we obtain Lebesgue measure on $[0, 1]$, and the corresponding polynomials are essentially the classical Legendre polynomials. (Actually, the classical Legendre polynomials are orthogonal with respect to Lebesgue measure on $[-1, 1]$ and are normalized differently, but the differences just involve rescaling the axes.) When $R = 2$ and $p_1 \neq p_2$, we refer to the corresponding polynomials

as *weighted Legendre polynomials* (WLP). (In other contexts, these are known as "biased coin" measures. See, for example, [Talagrand 89].)

The measure μ is singular but not supported on any proper closed subset of $[0, 1]$. When $R > 2$, we will always take $p_1 = p_2 = \frac{1}{2}$, and we call the corresponding polynomials *Cantor Legendre polynomials* (CLP). The measure μ is then supported on a Cantor set C_R characterized by

$$C_R = F_1C_R \cup F_2C_R.$$

The standard Cantor set and Cantor measure correspond to $R = 3$. We refer to the intervals in $[0, 1] \setminus C_R$ as gaps. The largest gap is the interval $(\frac{1}{R}, 1 - \frac{1}{R})$, and there are 2^m gaps of length $\frac{1}{R^{m-1}}(1 - \frac{2}{R})$.

The behavior of $P_n(x)$ in the CLP case is quite different on the gaps and on the Cantor set C_R. In order to visualize the graphs of $P_n(x)$ on C_R, we introduce the distorted Cantor set $\widetilde{C}_{R,\epsilon}$ (also known as the Smith–Volterra–Cantor set or fat Cantor set), obtained by reducing the size of the gaps by a factor of ϵ (a parameter that we choose). Note that $\widetilde{C}_{R,\epsilon}$ is still a topological Cantor set, but it has positive Lebesgue measure. There is an obvious one-to-one correspondence between C_R and $\widetilde{C}_{R,\epsilon}$ that identifies regions between corresponding gaps. We use this identification to graph functions defined on C_R against $\widetilde{C}_{R,\epsilon}$.

In Section 2 we present data for the entries of the Jacobi matrix. In the CLP case we note the different behaviors of r_n for even and odd n, and the occurrence of small values. In Section 3 we display graphs of the polynomials. In the CLP case we show graphs of the restrictions to the Cantor set and to the gaps.

We then discuss various features of the data. In Section 4 we discuss the associated Dirichlet kernels. Using the Christoffel–Darboux formula, we are able to relate approximate identity behavior with small values of r_n. In Section 5 we discuss some approximate equalities relating CLP restricted to the Cantor set. In particular, $P_{2n}(x)$ is approximately equal to $P_{2n+1}(x)$ on the right half of C_R, for large n.

We also define a "shuffle" map that approximately preserves P_{2n+1} when n is a power of 2. In Section 6 we discuss the behavior of $P_n(x)$ on the gaps in the CLP case. On the central gap, for high n, $P_n(x)$ vaguely approximates either a Gaussian or the derivative of a Gaussian, depending on $n \mod 2$. More precisely, we find that

$$P_{2n}(x) = c_{2n}e^{-d_{2n}x^{\alpha(x)}},$$

where $\alpha(x) = \alpha_{2n}(x) = 2$ at $x = 1/2$, and $\alpha(x) \approx 2$ for x around $1/2$. On the other gaps, for large enough n, the

behavior is roughly the same. In Section 7 we discuss the behavior of $P_n(x)$ at the points $x = 0, 1/4, 1/2, 3/4, 1$ in the WLP case, and we contrast the results with the known behavior for Legendre polynomials. This study leads to the dynamical systems perspective.

Instead of thinking of $P_n(x)$ as a function of x for fixed n, we look at $P_n(x)$ as a function of n, for a fixed x. Because of the 3-term recurrence relation, it is more natural to look at vectors $(P_n(x), P_{n+1}(x))$ in the plane. Then there exist 2×2 matrices $M_n(x)$ such that

$$\begin{pmatrix} P_{n+1}(x) \\ P_n(x) \end{pmatrix} = M_n(x) \begin{pmatrix} P_n(x) \\ P_{n-1}(x) \end{pmatrix}.$$

In fact,

$$M_n(x) = \begin{pmatrix} \frac{x - A_n}{r_{n+1}} & -\frac{r_n}{r_{n+1}} \\ 1 & 0 \end{pmatrix}.$$

So, we are really looking at orbits of a time-dependent linear dynamical system. We can then define the analog of the Mandelbrot set as all x for which the orbit is bounded. Then for each x in this Mandelbrot set, we can define a Julia set $J(x)$ as the limit set of the orbit. We display some examples of these Julia sets. We then extend the investigation of Section 7 to generic x for WLP and CLP in Section 8. We end with a short concluding discussion in Section 9.

This paper should be viewed in the context of a long-term effort to understand topics in classical analysis extended to fractal measures. The following references are just a sampling of this work: [Bird et al. 06, Coletta et al. 04, Dutkay and Jorgensen 06, Huang and Strichartz 01, Jorgensen and Pedersen 00, Kigami 01, Laba and Wang 02, Lau and Wang 93, Lund et al. 98, Strichartz 90, Strichartz 93a, Strichartz 93b, Strichartz 94, Strichartz 98, Strichartz 00, Strichartz 05, Strichartz 06]. More data may be found at www.math.cornell.edu/ orthopoly.

2. ENTRIES OF THE JACOBI MATRIX

The coefficients r_n and A_n in the 3-term recurrence relation (1–1) determine the polynomials in a rather subtle way. More work is needed to clarify this relationship. In this section we report data for our two classes of examples. In Figures 1–4 we graph A_n and r_n versus n, for several choices of p_1 in the WLP case. For classical Legendre polynomials we have $A_n = 1/2$ for all n by symmetry about $x = 1/2$, and $\lim_{n \to \infty} r_n = 1/4$. The WLP case shows a small but significant difference from this model case.
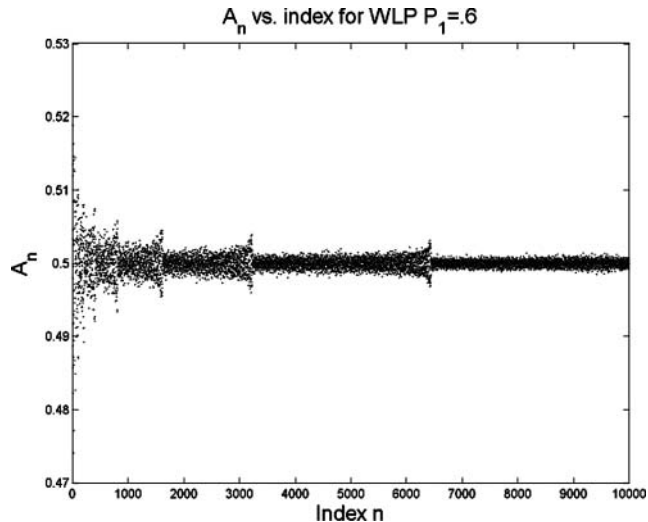

FIGURE 1. Plot of A_n vs. index n, $1 \le n \le 10000$ for $p_1 = 0.6$

In the CLP case, all A_n are equal to $1/2$ by symmetry about $x = 1/2$. In Figure 5 we graph r_n versus n for $R = 8$.

Problem 2.1. What is the nature of the limit set

$$\bigcap_{N=1}^{\infty} \text{cl} \left(\bigcup_{n=N}^{\infty} \{r_n\} \right)?$$

Do the measures

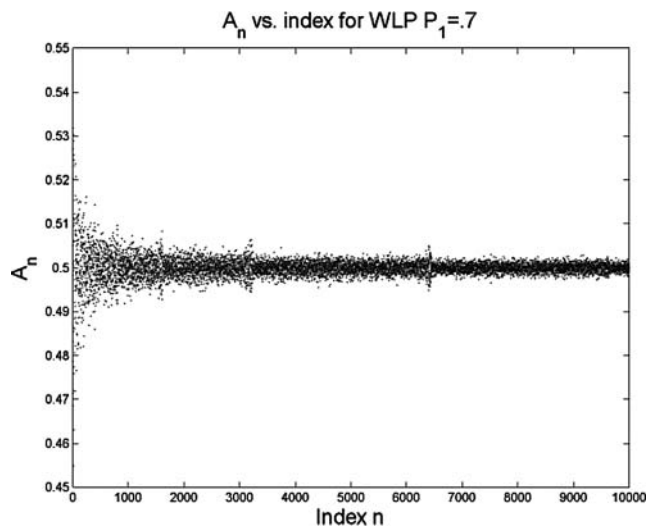$$\frac{1}{m-k} \sum_{n=k+1}^{m} \delta_{r_n}$$

FIGURE 2. Plot of A_n vs. index n, $1 \le n \le 10000$ for $p_1 = 0.7$.
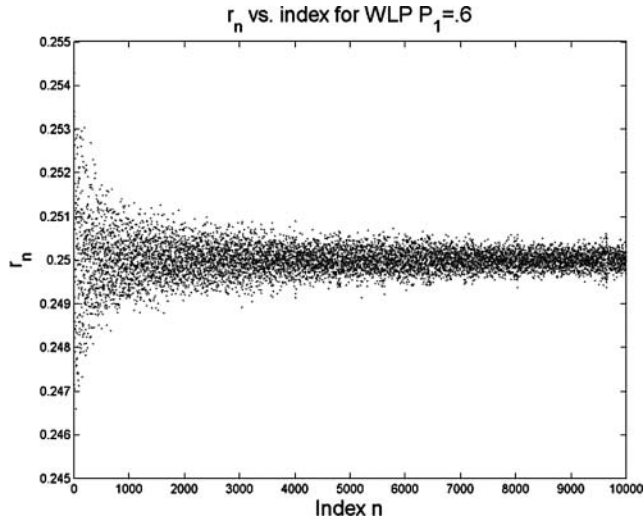
FIGURE 3. Plot of r_n vs. index n, $1 \leq n \leq 10000$ for $p_1 = 0.6$.
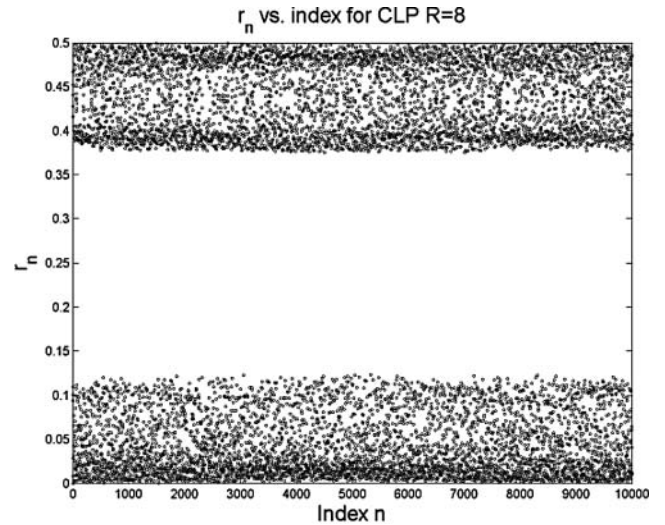

FIGURE 5. Plot of r_n vs. index n, $1 \leq n \leq 10000$ for CLP, $R = 8$.

converge weakly to some fractal measure as m, k tend to infinity in some specific manner?

A striking feature of the data is the different behavior of r_n for n even and n odd. In Figures 6 and 7 we show the same data as in Figure 5, separating the even and odd values of n. Another striking observation is that some values of r_n for n even are close to zero.

Problem 2.2. What is

$$\liminf_{n \to \infty} r_n ?$$

In particular, is the $\liminf$ zero? What is the sequence of n's along which the $\liminf$ is attained?

As we will see later, having values of r_n close to zero has interesting implications. We could also ask for the $\limsup$, but it is not clear what significance this has.

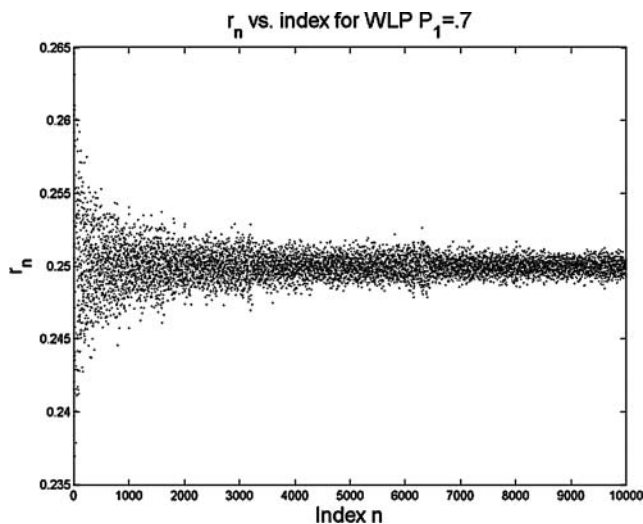**Conjecture 2.3.** *We always have*

$$r_n \leq \frac{1}{2}.$$

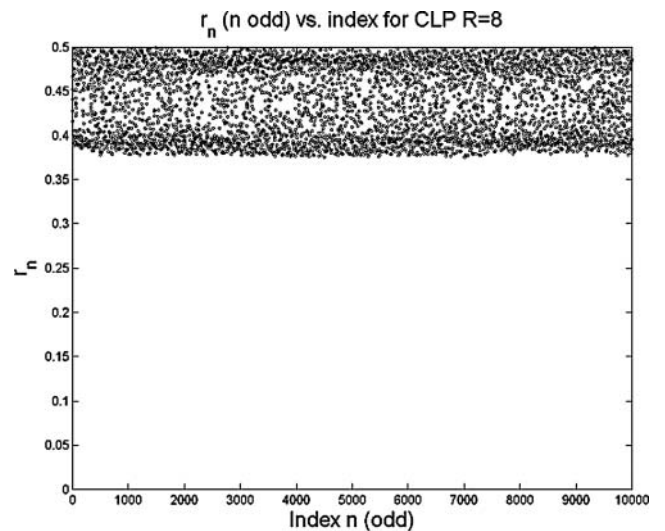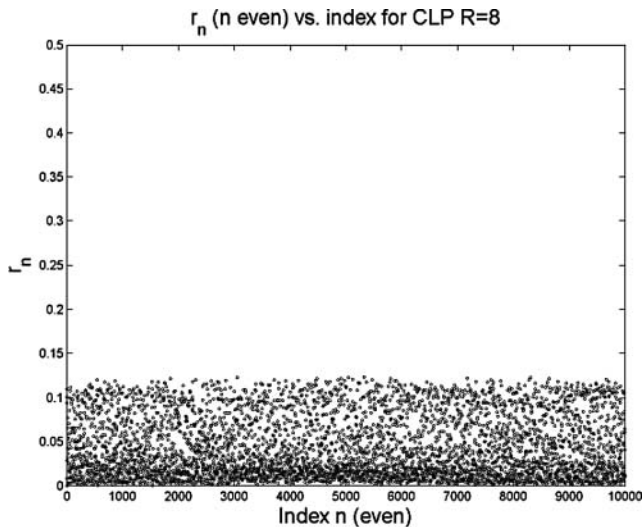**FIGURE 4.** Plot of r_n vs. index n, $1 \leq n \leq 10000$ for $p_1 = 0.7$.

FIGURE 6. Plot of r_n vs. index n, $1 \leq n \leq 10000$ for n odd, CLP, $R = 8$.

FIGURE 7. Plot of r_n vs. index n, $1 \leq n \leq 1000$ for n even, CLP, $R = 8$.

Let us now review some rigorous results on the coefficients A_n and r_n. As stated above, for the Legendre polynomials (on $[0,1]$), we have $A_n = 1/2$ and $\lim r_n = 1/4$. Any measure satisfying $\lim A_n = 1/2$ and $\lim r_n = 1/4$ is said to be in Nevai's class $M(\frac{1}{2}, \frac{1}{4})$. By Blumenthal's theorem, any $\mu \in M(\frac{1}{2}, \frac{1}{4})$ has support $[0,1]$ along with at most countably many other points, which can accumulate only at the endpoints $x = 0$, $x = 1$. (See [Máté et al. 91, Theorem 10]. This theorem is a special case of Hermann Weyl's theorem on compact perturbations of self-adjoint operators on Hilbert spaces.)

For CLP, note that $A_n = 1/2$ by symmetry, so (the contrapositive of) Blumenthal's theorem implies that r_n cannot converge to $1/4$. And Figures 5–7 concur. However, some weaker conditions do in fact hold. For CLP and WLP, A_n and r_n converge in Cesàro mean [Fischer 95]. (A sequence $\{b_n\}_0^\infty$ converges in Cesàro mean if $\frac{1}{N} \sum_{i=0}^{N-1} b_n$ converges.) This convergence in Cesàro mean follows because CLP and WLP are defined by regular measures, to use the terminology of (logarithmic) potential theory. For a proof that the CLP measures are regular, see [Fischer 95, Theorem 1 and Lemma 2].

According to one's interpretation of Figures 1-4, WLP may or may not be in $M(\frac{1}{2}, \frac{1}{4})$. Nevertheless, something stronger than convergence in Cesàro mean is known: A_n and r_n converge in density to $\frac{1}{2}$ and $\frac{1}{4}$, respectively. We say that $\{b_n\}$ converges in density to b if for all $\delta > 0$,

$$\limsup_{n \to \infty} \frac{1}{n} \#\{k : k \leq n, |b_k - b| > \delta\} = 0.$$

As with the previous convergence result, this one can be obtained from general assumptions. Since the WLP measures are regular and their support is the entire interval $[0,1]$, the convergence in density result follows; see [Fischer 95, Theorem 2]. It remains to improve upon these results.

3. GRAPHS OF POLYNOMIALS

In Figure 8 we show the graphs of $P_n(x)$ for $1 \leq n \leq 5$ for the WLP with $p_1 = 1/2$, so these are just (rescaled versions of) the classical Legendre polynomials, computed using G. Mantica's algorithm. In Figures 9 and 10 we show the same functions for $p_1 = 0.6$ and $p_1 = 0.7$. Already we observe that the symmetry is broken in a decisive fashion, since these functions are much larger near $x = 1$ (where the measure "has less weight") than near $x = 0$ (where the measure "has more weight").

This observation is expected, since the Gram–Schmidt process with respect to μ almost immediately implies the following property: $P_n(x)$ is the unique nth-degree polynomial with highest-degree coefficient d_n that minimizes the $L^2([0,1], \mu)$ norm. In the case $p_1 = 1/2$, we have

$$d_n = \prod_{i=1}^n \frac{1}{b_i} \quad \text{and} \quad 1/b_i = \sqrt{16 - 4/i^2}.$$

Therefore, P_n is expected to be the smallest where μ "has more support." In Figure 11 we show the graphs of $P_n(x)$ for $49 \leq n \leq 52$ for $p_1 = 0.7$. The same graphs are shown in Figure 12 with the y-axis truncated to display the structure of the functions more clearly. These figures lead us to the following problem:

Problem 3.1. For fixed $p_1 > 1/2$ and any given $\epsilon > 0$, what is the growth rate of $\max_{x \in [\epsilon, 1-\epsilon]} |P_n(x)|$ for WLP?

By [Stahl and Totik 92, Theorem 3.1.1(iii)], we know that $\limsup |P_n(x)|^{1/n} = 1$ on $[0,1]$, possibly excluding sets of capacity zero. Recall that the capacity $\text{cap}(K)$ of a compact set K is defined as

$$\text{cap}(K) = \exp\left(-\inf_{S(\nu) \subset K} \iint \log \frac{1}{|z - t|} d\nu(z) d\nu(t)\right),$$

where

$$S(\nu) = \text{supp}(\nu) = \{x : \nu([x - \delta, x + \delta]) > 0, \forall \delta > 0\}.$$

As a result, if we fix $x \approx 1$ and increase n, then $|P_n(x)|$ may have polynomial growth in n, but not exponential growth. Discerning the exact growth of $|P_n(x)|$ seems difficult, but we make some effort toward this goal in
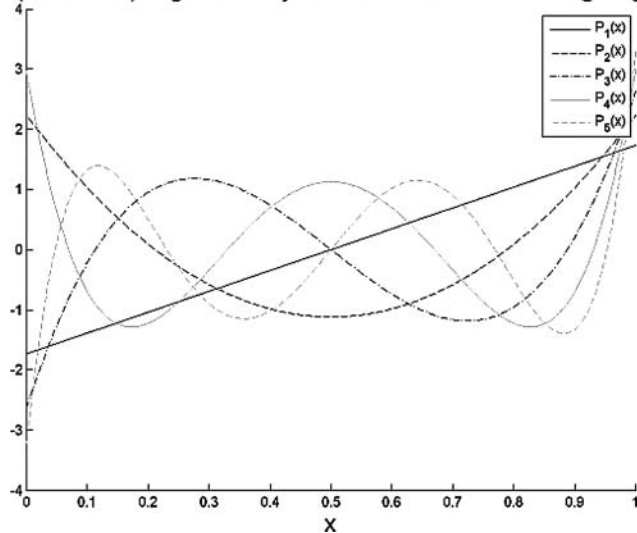
p_1	$\epsilon = 0.1$	$\epsilon = 0.01$	$\epsilon = 0.001$
0.6	$*$	0.1	0.15
0.7	0.3	0.25	0.3
0.8	0.6	0.44	0.8
0.9	1.1	0.76	1.3

TABLE 1. Order of growth $n^{(\cdot)}$ of $\max_{x \in [\epsilon, 1-\epsilon]} |P_n(x)|$. Experimentally determined orders of growth. An entry of α means that for a certain ϵ and p_1, we have $\max_{x \in [\epsilon, 1-\epsilon]} |P_n(x)| \approx n^\alpha$. The star symbol $(*)$ indicates a very slow order of growth, which could be a polynomial of very small degree, or logarithmic growth.

Table 1. Here, we examine the function $\max_{x \in [\epsilon, 1-\epsilon]} |P_n(x)|$ for WLP with different p_1 and ϵ values. We see that this function typically has very slow logarithmic or polynomial growth. Note that we have chosen the interval $[\epsilon, 1-\epsilon]$, because the maximum of $|P_n(x)|$ for WLP typically occurs near the points $x = 0$ and $x = 1$. However, as Figure 34 demonstrates, $P_n(0)$ becomes bounded in n, for $p_1 > p \approx 0.7$. This observation suggests that we could have instead analyzed the interval $[0, 1-\epsilon]$ for such values of p_1.
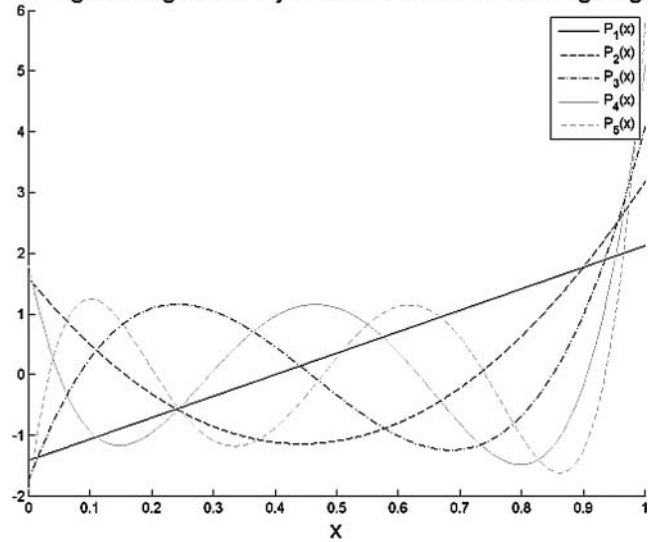
Next we look at the CLP case, where certain features of the $P_n(x)$ increase in complexity. In Figures 13 and 14 we show the graphs of $P_n(x)$ for $1 \le n \le 5$ on the whole

FIGURE 9. Plot of $P_n(x)$ on the unit interval with $p_1 = 0.6$, $p_2 = 0.4$. Recall that the 60 percent weighting is given to the map which contracts towards zero.

interval for two different choices of R. In Figure 15 we show the graph of $P_{52}(x)$ on the whole interval for $R = 4$. Note that the values on the central gap are so large that no information about the graph on the complement of the central gap is discernible using linear scaling in the y-axis. This is typical of $P_n(x)$ for large even values of $n = 2k$ and any $R > 2$ (though the $P_n(x)$ changes sign between $n = 4j + 2$ and $n = 4j$).

FIGURE 8. Plot of $P_n(x)$ on the unit interval with $p_1 = p_2 = 0.5$. This gives the classical Legendre Polynomials (up to renormalization).
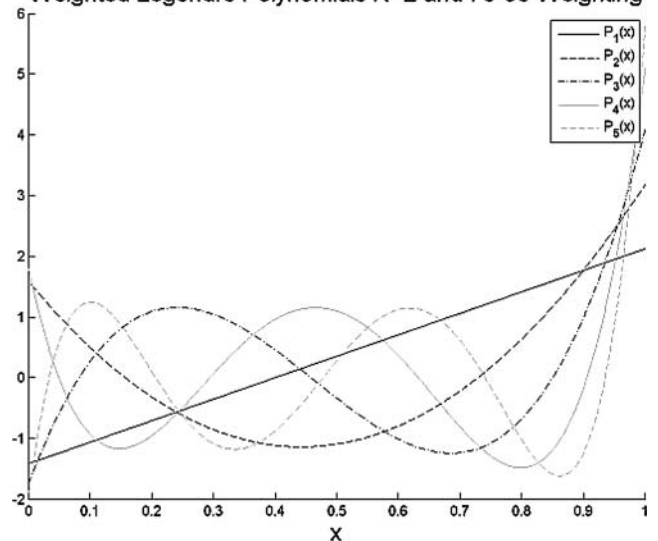

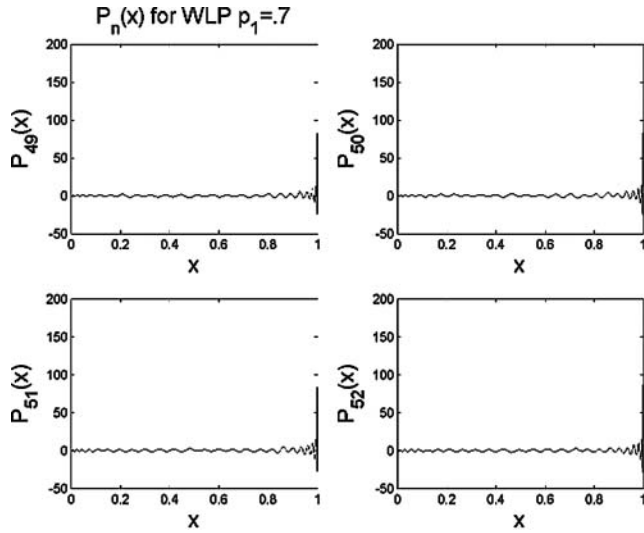**FIGURE 10.** Plot of $P_n(x)$ on the unit interval with $p_1 = 0.7$, $p_2 = 0.3$.

FIGURE 11. Plot of $P_n(x)$ on the unit interval with $p_1 = 0.7$, $p_2 = 0.3$ for $49 \leq n \leq 52$.

To view these polynomials more effectively, we scale the y-axis logarithmically, but also multiply by the sign of $P_n(x)$. That is, we plot $\text{sign}(P_n(x)) \log(|P_n(x)|)$ vs. x. In Figure 16 we show the graph of $P_{51}(x)$ for $R = 4$, which is typical of $P_n(x)$ for n odd and large. With the same logarithmic scaling, Figure 17 shows $P_{52}(x)$ for $R = 4$ restricted to the gap $[1/R^2, (R-1)/R^2] = [1/16, 3/16]$. This behavior is typical of $P_n(x)$ for large n. Note that the maximum value is quite large, but still it is small relative to the maximum value on the central gap. We will discuss this behavior more in Section 6.
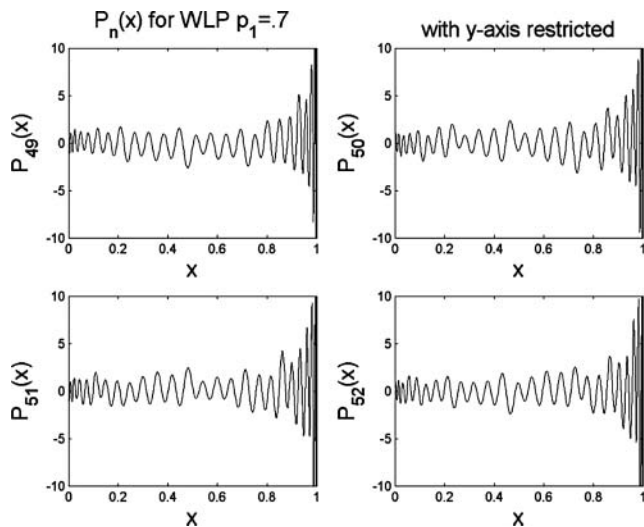

FIGURE 12. Plot of $P_n(x)$ on the unit interval with $p_1 = 0.7$, $p_2 = 0.3$ for $49 \leq n \leq 52$ with the y-axis restricted to the range $-10 \leq y \leq 10$.
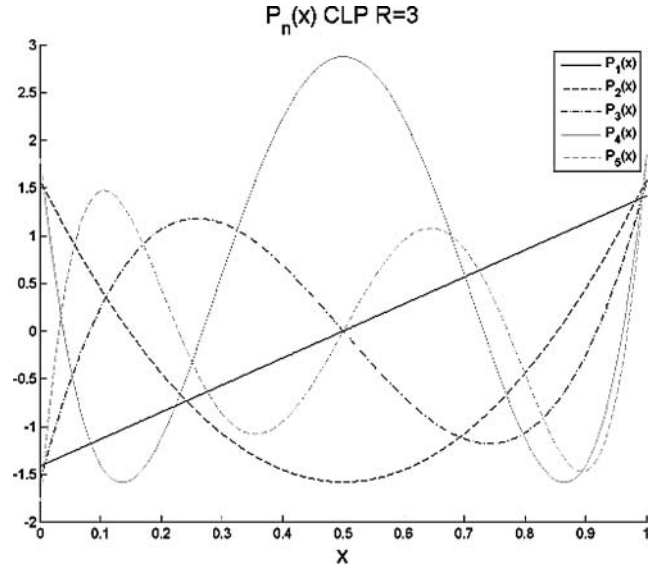

FIGURE 13. Plot of first five Cantor Legendre polynomials, $R = 3$.

Next, we graph CLP on the Cantor set C_R using a distorted Cantor set $\widetilde{C}_{R,\epsilon}$ for the x-axis. In Figures 18 and 19 we display the same functions as in Figures 13 and 14. Already we see that the values of $P_n(x)$ are considerably smaller on the Cantor set. In Figure 20 we show $P_n(x)$ restricted to the Cantor set for $97 \leq n \leq 100$ and $R = 8$. We will comment in detail about some of the structure
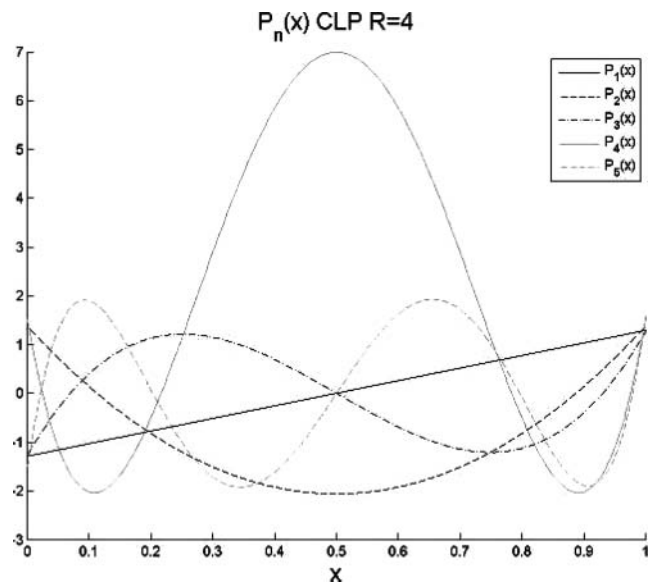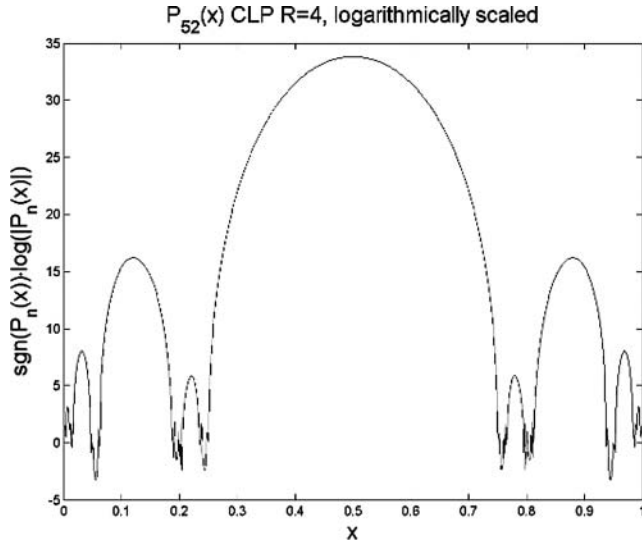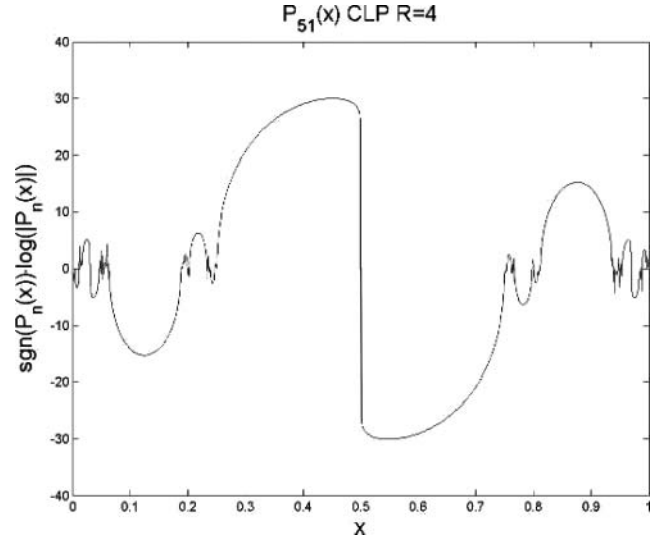

FIGURE 14. Plot of first five Cantor Legendre polynomials, $R = 4$. As in the Cantor Legendre case, the polynomials have lowest absolute value where the measure has the most weight (as expected).

FIGURE 15. Plot of $P_{52}(x)$ for CLP $R = 4$, logarithmically scaled on the entire interval. Notice the large values obtained by the polynomials off the Cantor set (10^{28}) compared to the behavior on the Cantor set (for $1 \leq j \leq n$ large, $|P_n| < 20$). The overall shape in the gap is Gaussian, and this occurs for all $n = 4k$, $k \in \mathbb{Z}^+$. For $n = 4k + 2$, the behavior in the gap is roughly a negative Gaussian.

of those graphs in Section 5. Many more examples may be viewed at [Owrutsky 05].

4. DIRICHLET KERNELS

For a general function f in $L^2(d\mu)$, we can expand it as a series

$$\sum_{n=0}^{\infty} a_n P_n(x),$$

where the coefficients are given by

$$a_n = \int f(y) P_n(y) \, d\mu(y).$$

The partial sums

$$\sum_{n=0}^{N} a_n P_n(x) \qquad (4\text{--}1)$$

may be represented as an integral

$$\int D_N(x, y) f(y) \, d\mu(y),$$

where the Dirichlet kernel is given by

$$D_n(x, y) = \sum_{n=0}^{N} P_n(x) P_n(y). \qquad (4\text{--}2)$$

FIGURE 16. Plot of $P_{51}(x)$ for CLP $R = 4$, logarithmically scaled on the entire interval. This is roughly the derivative of a Gaussian on the center gap. For all $n = 4k + 3$ we observe this shape, and for $n = 4k + 1$, the negative of this shape (color figure available online).

The partial sums in (4–1) converge to f in L^2 norm, but to get better convergence we need to know more about the Dirichlet kernel. In view of related results in [Strichartz 93b, Strichartz 94], one might hope that there exists a sequence $\{N_k\}$ along which the partial sums converge uniformly if f is continuous. This would follow by standard approximate identity arguments if we could
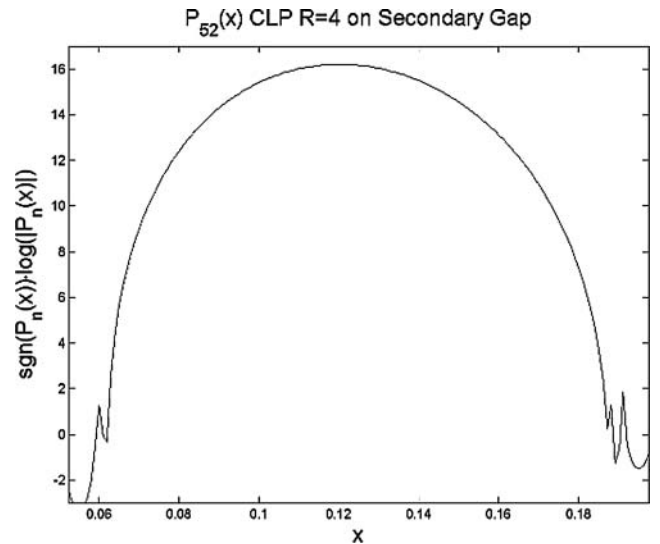
FIGURE 17. Plot of $P_{52}(x)$ for CLP $R = 4$, logarithmically scaled on the secondary gap $[1/R, (R-1)/R] = [1/16, 3/16]$. Again, we observe a Gaussian shape.
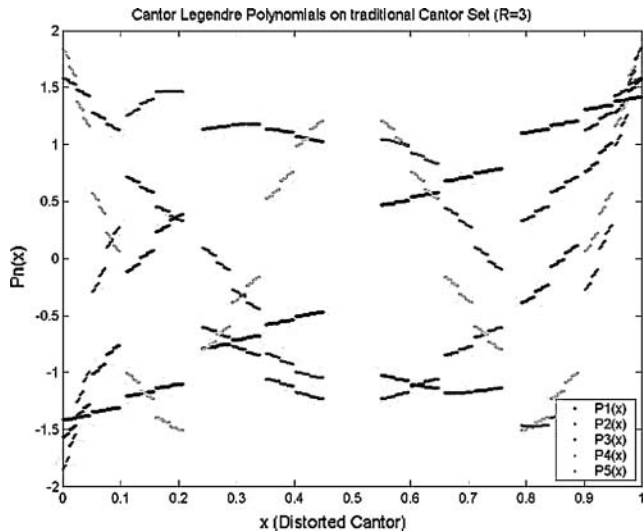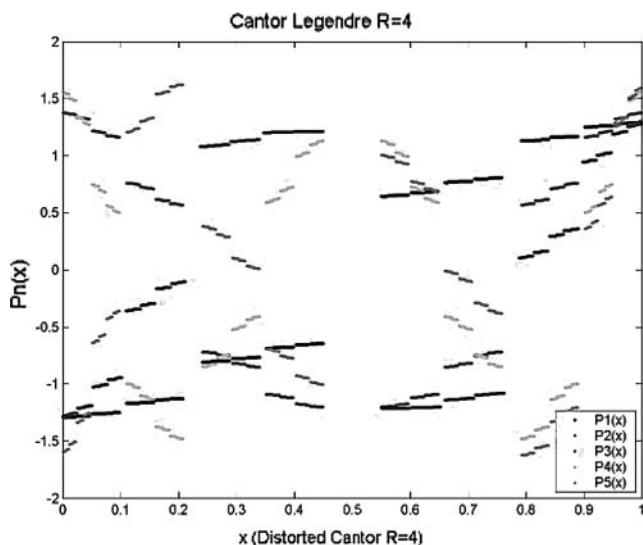
FIGURE 18. Plot of first five Cantor Legendre polynomials, $R = 3$.

FIGURE 20. Plot of some larger n Cantor Legendre polynomials, $R = 8$, $97 \le n \le 100$.

show that the quantity

$$\int |D_{N_k}(x,y)| \, d\mu(y) \qquad (4\text{--}3)$$

is uniformly bounded, and that

$$\lim_{k \to \infty} \int_{|y-x| \ge \epsilon} |D_{N_k}(x,y)| \, d\mu(y) = 0 \qquad (4\text{--}4)$$

for all $\epsilon > 0$. While we have no insight on how to establish (4–3), we can say something about (4–4), thanks to the

Christoffel–Darboux formula

$$D_N(x,y) = \frac{r_{N+1}}{x-y}(P_{N+1}(x)P_N(y) - P_N(x)P_{N+1}(y)), \qquad (4\text{--}5)$$

for $x \ne y$. (It is easy to derive (4–5) by multiplying (4–2) by $(x - y)$ and using the 3-term recurrence relation (1–1).) Assuming that the polynomials $P_n(x)$ are uniformly bounded on the support of μ, if we could find a sequence N_k such that $r_{N_{k+1}} \to 0$, then (4–4) would follow from (4–5).

It appears from our data that for CLP polynomials there exist indices n such that r_n is close to zero, but there is no evidence for a sequence tending to zero. This means that there will be some Dirichlet kernels that seem very concentrated near the diagonal (those with r_{N+1} close to zero), but it is unlikely that we can improve this behavior indefinitely.

Figures 21 and 22 illustrate Dirichlet kernels $D_N(\cdot, y)$ for fixed y that are not concentrated near $x = y$, while Figures 23 and 24 illustrate Dirichlet kernels that are moderately well concentrated.

5. APPROXIMATE EQUALITIES FOR CLP POLYNOMIALS

In this section we discuss two types of approximate equalities in the CLP case. First we note that by symmetry, $P_n(x)$ is even under the reflection $x \mapsto 1 - x$ when n is even, and odd when n is odd. Nevertheless, the plots of $P_{2n}(x)$ and $P_{2n+1}(x)$ appear very similar (see $n = 98, 99$

FIGURE 19. Plot of first five Cantor Legendre polynomials, $R = 4$.
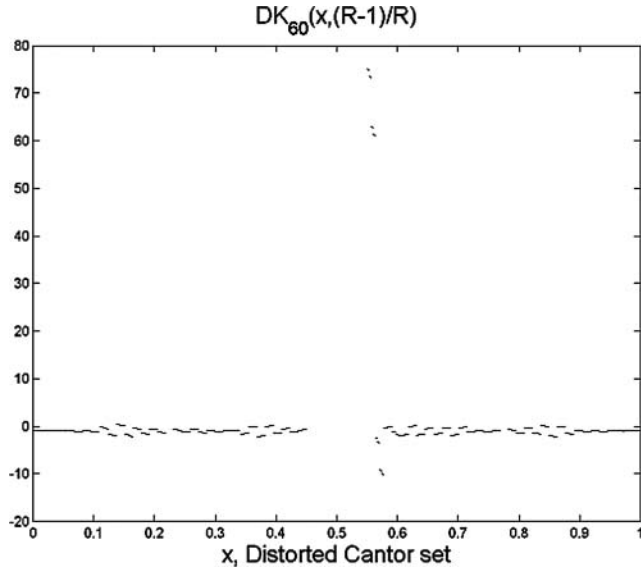
FIGURE 21. Dirichlet kernel for CLP with $n = 60$ and $R = 8$ centered at the leftmost point in the right half of the Cantor set. We see that the graph is reasonably small away from the center.
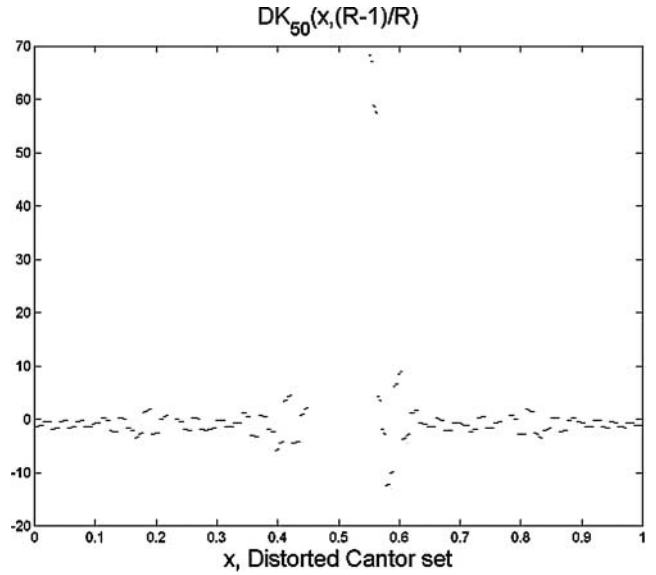
FIGURE 23. Dirichlet kernel for CLP with $n = 50$ and $R = 8$ centered at the leftmost point in the right half of the Cantor set. This kernel takes much larger values away from the center than the $n = 60$ case in Figure 21.

in Figure 20). This is especially true on the right half of the Cantor set. In Figure 25 we graph $P_{50}(x)$ and $P_{51}(x)$ for $R = 8$.

The qualitative similarity is striking, but it is difficult to quantify. Figure 26 shows the graph of the difference, and Figure 27 shows the graph of the ratio. We can give

a rough explanation using (1–2), which for even values may be written

$$P_{2n+1}(x) = \frac{x - 1/2}{r_{2n+1}} P_{2n(x)} - \frac{r_{2n}}{r_{2n+1}} P_{2n-1}(x). \quad (5\text{--}1)$$

For large values of R, we may have r_{2n} close to zero and r_{2n+1} close to $1/2$. So the second term on the
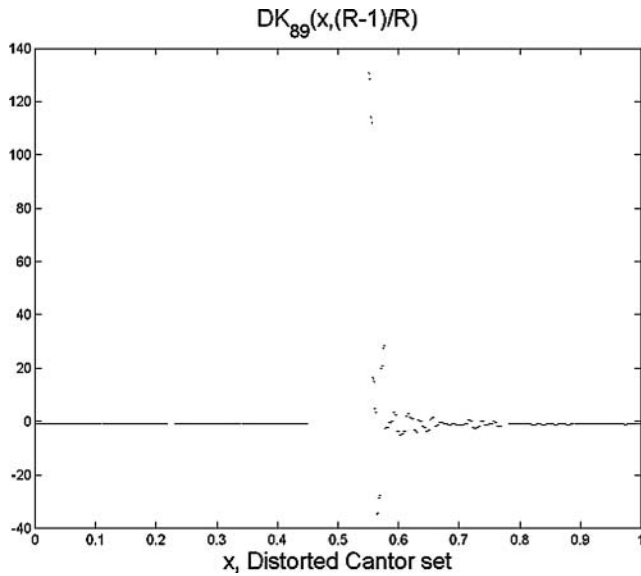
FIGURE 22. Dirichlet kernel for CLP with $n = 89$ and $R = 8$ centered at the leftmost point in the right half of the Cantor set. Again, the kernel is small away from its center.
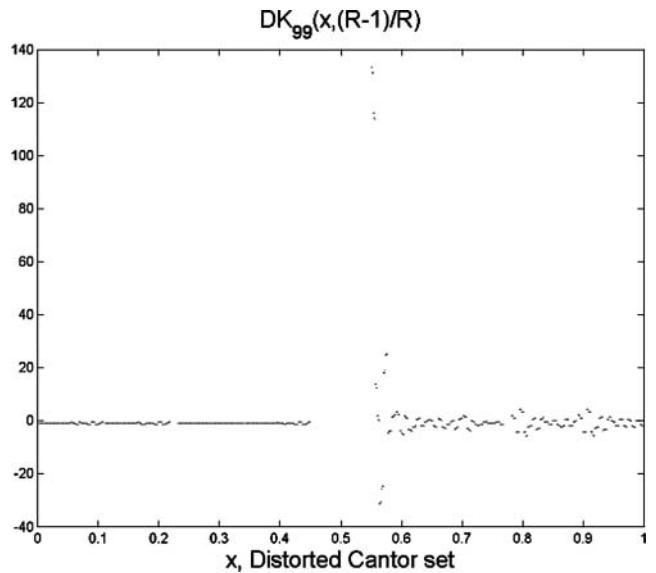
FIGURE 24. Dirichlet kernel for CLP with $n = 99$ and $R = 8$ centered at the leftmost point in the right half of the Cantor set.

FIGURE 25. $P_{80}(x)$ and $P_{81}(x)$, CLP $R = 8$.

FIGURE 27. $P_{80}(x)/P_{81}(x)$, CLP $R = 8$.

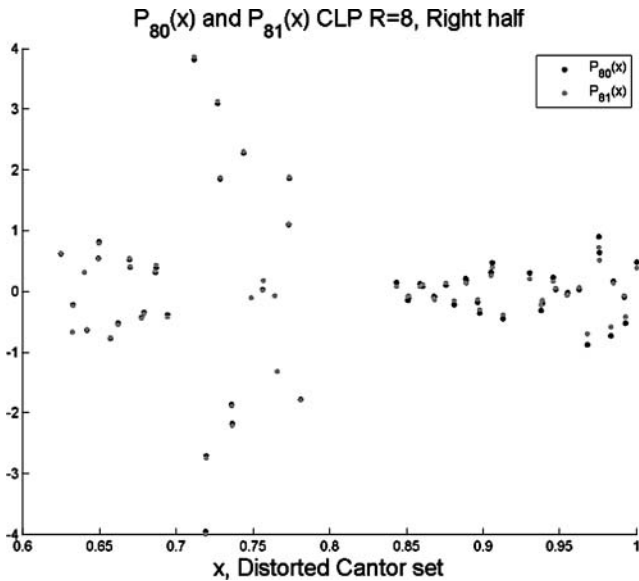right-hand side of (5–1) is close to zero. But on the right half of the Cantor set, x is close to one, so the coefficient $(x - 1/2)/r_{2n+1}$ is close to one. Therefore, (5–1) says that $P_{2n+1}(x) \approx P_{2n}(x)$ on the right half of C_R.

By the odd–even behavior, we have $P_{2n+1}(x) \approx -P_{2n}(x)$ on the left half of C_R. Since we see a qualitative similarity among the plots on all of C_R, we must attribute these approximate equalities to an approximate reflectional symmetry across the x-axis of the graphs of all $P_n(x)$. This is roughly apparent in Figure 20, but it

does not hold up to close inspection. In particular, the graphs of $P_{2n+1}(x)$ and $P_{2n+1}(1 - x)$ are not that close (of course $P_{2n+1}(1 - x) = -P_{2n+1}(x)$ exactly).

The second type of approximate equality refines the above idea. If we express the points of C_R as infinite binary decimals, then $x \mapsto (1 - x)$ simply interchanges all digits in the binary expansion. Let $T_m(x)$ denote the map $C_R \to C_R$ that interchanges the first m binary digits, leaving all other digits unchanged. In other words, T_m permutes the 2^m Cantor subsets of level m by reversing the order of the subsets. In Figure 28 we show the plots of $P_{17}(x)$ and $P_{17}(T_3(x))$ for $R = 8$. There is

FIGURE 26. $P_{80}(x) - P_{81}(x)$, CLP $R = 8$.

FIGURE 28. $P_{17}(x)$ and $P_{17}(T_3(x))$, $R = 8$.

FIGURE 29. $\alpha(x)$ for CLP $R = 4$, $n = 50$.

clearly a strong qualitative fit, but the agreement of the two functions is not very close numerically. The same pattern persists for $P_{2^m+1}(x)$ and $P_{2^m+1}(T_m(x))$ for all values of R. At present we have no explanation for this phenomenon.

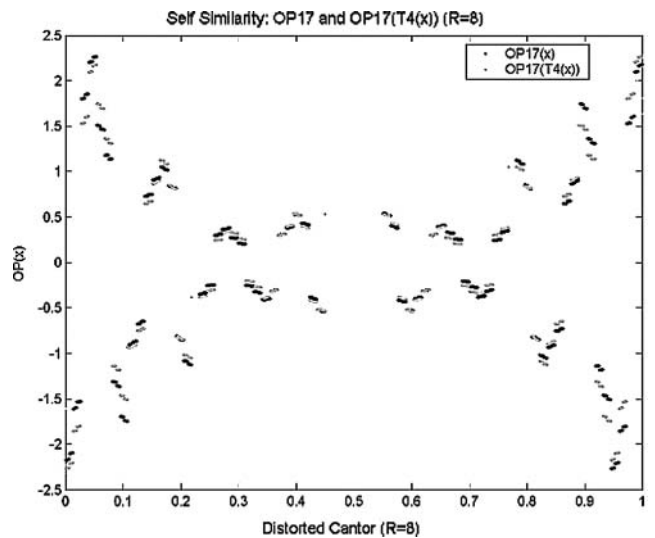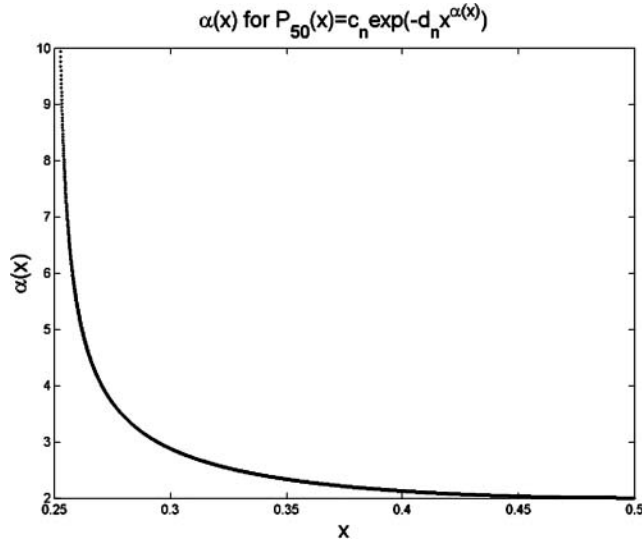## 6. CLP POLYNOMIALS ON GAPS

We saw in Figures 15 and 17 that the graph of $P_{2n}(x)$ on the gaps in C_R is approximately Gaussian, for n large. In reality, we find that $P_{2n}|_{[1/R,(R-1)/R]}(x) =$

$c_{2n} \exp\left(-d_{2n}x^{\alpha(x)}\right)$, where $\alpha(x) = \alpha_{2n}(x) = 2$ at $x = 1/2$, and $\alpha(x) \approx 2$ for x around $1/2$. Figure 29 shows $\alpha(x) = \alpha_{2n}(x)$ for $n = 50$, CLP $R = 4$. Due to symmetry, we view α only on the interval $[1/R, 1/2]$. From the data, we conjecture that α_{2n} converges as $n \to \infty$ on any closed interval of the form $[1/R + \epsilon, 1/2]$ to a function resembling that in Figure 29.

The data also indicate exponential growth (in n) of $P_{2n}(x)$ on the central gap $[1/R, (R-1)/R]$. This exponential growth results from the behavior of (1–2) at $x = 1/2$ (with $A_n = 1/2$ for all n) as follows:

$$P_{2n}(1/2) = (-1)^n \prod_{j=1}^{n}(r_{2j-1}/r_{2j}). \qquad (6\text{--}1)$$

Numerically, we find that (r_{2j-1}/r_{2j}) is bounded above 1 with few exceptions. In the CLP $R = 2.5$ case, there are 134 instances in which $(r_{2j-1}/r_{2j}) \leq 1$ for $j = 1, \ldots, 5000$; in the $R = 3$ case, there is one; and for the $R = 4$ case, there are none. Thus, as R increases, (r_{2j-1}/r_{2j}) is bounded above 1 more consistently, as we have seen in the $R = 8$ case in Figures 6 and 7. Therefore, (6–1) (generally) gives exponential growth in n for $|P_{2n}(1/2)|$.

We then summarize the behavior of $P_{2n}(x)$ on the gap $[1/R, (R-1)/R]$ as follows: $c_{2n} = P_{2n}(1/2)$ grows exponentially (according to (6–1), d_{2n} grows linearly, and $\alpha_{2n}(x)$ appears to converge, to something resembling
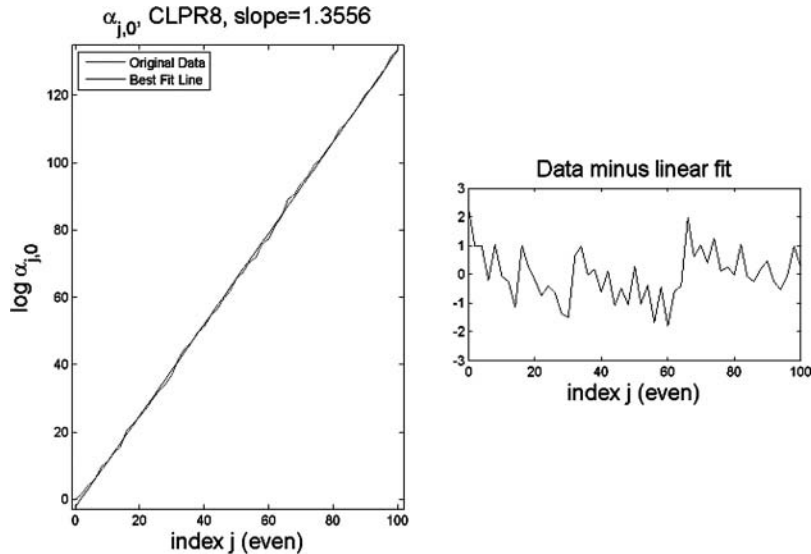

FIGURE 30. Logarithmically scaled left column $\{\alpha_{j,0}\}$ of polynomial coefficients, with error, CLP $R = 8$. Here we only plot j even since for odd j, $\alpha_{j,0} = 0$.
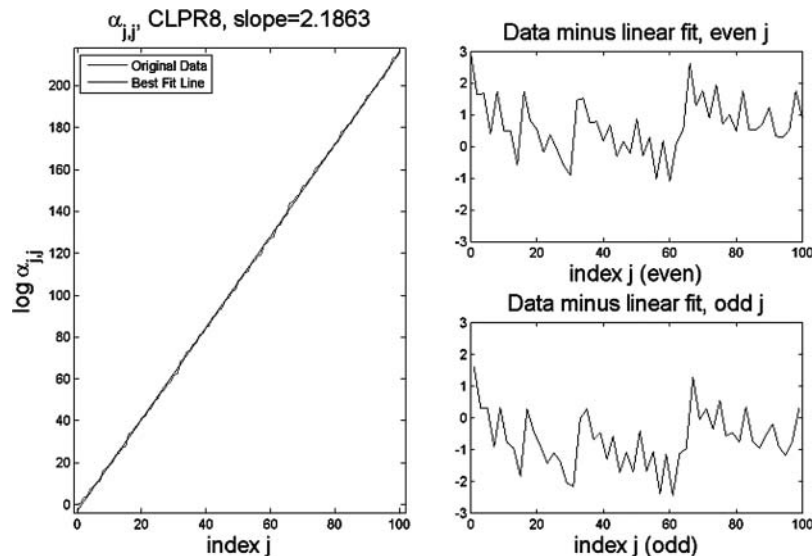
FIGURE 31. Logarithmically scaled diagonal $\{\alpha_{j,j}\}$ of polynomial coefficients, with error, CLP $R = 8$.

Figure 29). In fact, we can say more: for $k \in \mathbb{Z}^+$, write

$$P_j(x) = \sum_{k=0}^{j} \alpha_{j,k}(x - 1/2)^k.$$

Equation (6–1) gives all $\alpha_{j,0}$ (observe that $\alpha_{2n,0} = c_{2n}$ and $\alpha_{2n+1,0} = 0$ for all n), and then we can again use (1–2) to compute all of the $\alpha_{j,k}$. (Here we read (1–2) as an equation of polynomials.) If we view the coefficients $\{\alpha_{j,k}\}$ as a (lower triangular) matrix, then we see that the left column $\{\alpha_{j,0}\}$ and the diagonal $\{\alpha_{j,j}\}$ determine all of the other $\alpha_{j,k}$, via (1–2). Thus, the behavior of the

left column and diagonal (and the r_j coefficients) dictates the behavior of the other $\alpha_{j,k}$.

The left column and diagonal grow log-linearly, as we see in Figures 30 and 31 and Table 2. Note the similarity in the three error plots of Figures 30 and 31. If we label the (top) even-indexed error Φ_{even}, the (bottom) odd error Φ_{odd}, and the (even) error function from Figure 30 Ψ_{even}, we have the following approximate equalities for $k = 0, \ldots, 50$: $\Phi_{\mathrm{even}}(2k) \approx \Phi_{\mathrm{odd}}(2k + 1) + 1.36 \approx \Psi_{\mathrm{even}}(2k) + 0.67$. Also, from Table 2 we see that $\mathrm{sign}(\alpha_{j,k}) = -\mathrm{sign}(\alpha_{j,k+2})$, for appropriate j, k. For the

$\alpha_{j,k}/10^4$	0	1	2	3	4	5	6	7	8	9	10
0	0.0001	0	0	0	0	0	0	0	0	0	0
1	0	0.00022678	0	0	0	0	0	0	0	0	0
2	−0.00040311	0	0.0020732	0	0	0	0	0	0	0	0
3	0	−0.0010002	0	0.0048457	0	0	0	0	0	0	0
4	0.0061259	0	−0.067032	0	0.17212	0	0	0	0	0	0
5	0	0.013607	0	−0.14851	0	0.38055	0	0	0	0	0
6	−0.027586	0	0.43733	0	−2.2537	0	3.789	0	0	0	0
7	0	−0.069611	0	1.0873	0	−5.5105	0	9.1099	0	0	0
8	1.4436	0	−31.645	0	254.75	0	−891.62	0	1146.2	0	0
9	0	3.0921	0	−67.772	0	545.53	0	−1909.1	0	2454.1	0
10	−7.2086	0	191.07	0	−1996.6	0	10284	0	−26134	0	26237

TABLE 2. CLP $R = 8$, matrix of (rounded) $\alpha_{j,k}$ coefficients, divided by 10^4.
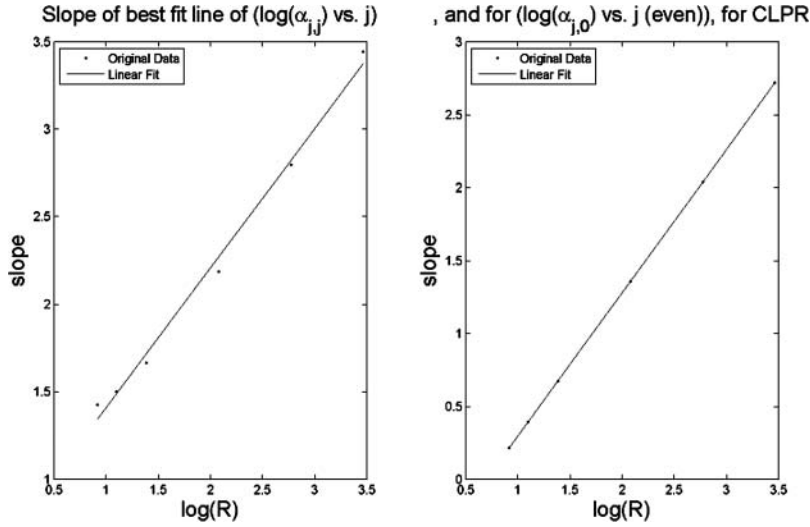
FIGURE 32. Slopes of best fit lines for $\alpha_{j,j}$ on the left and $\alpha_{j,0}$ on the right (as in Figures 30 and 31), for $R \in \{2.5, 3, 4, 8, 16, 32\}$.

column and the diagonal of the matrix of $\alpha_{j,k}$, the slope of each best-fit line varies with $\log R$, as we see in Figure 32.

On the other gaps (i.e., the images of $[1/R, (R-1)/R]$ under compositions of the maps F_1 and F_2), we observe similar qualitative behavior. That is, on these smaller gaps, $P_n(x)$ resembles a Gaussian for all large and even n. We have seen this self-similar behavior already in Figures 15 and 16. However, the local extremum of $P_{2n}(x)$ on $[1/R^2, (R-1)/R^2]$ is not in general the center of the given gap. We glimpse this phenomenon in Figure 17. In Figure 33 we plot the local extremum of $P_{2n}|_{[1/16,3/16]}$ in the CLP $R = 4$ case. The center of this gap occurs at $x = 0.125$, but the local extremum fluctuates with average around 0.122.

Let us briefly mention some rigorous results that reinforce these observations. As stated above, the CLP measures are regular, in the sense of (logarithmic) potential theory. Let $z \in \mathbb{C}$ and consider the polynomials $P_n(z)$ extended to the complex plane. Thus, for a CLP measure μ, [Stahl and Totik 92, Theorem 3.1.1(ii)] says that

$$\lim_{n \to \infty} |P_n(z)|^{1/n} \tag{6–2}$$
$$= \exp(-\log \operatorname{cap}(S(\mu)) + \int d\omega(z) \log(z - x))$$

locally uniformly in $\mathbb{C} \cup \{\infty\} \setminus [0, 1]$. That is, for fixed $z \in \mathbb{C} \cup \{\infty\} \setminus [0, 1]$, if $z_n \to z$, then $P_n(z_n)$ approaches the right-hand side of (6–2), as $n \to \infty$. Here, ω is the equilibrium measure for the Cantor set $S(\mu) = \operatorname{supp}(\mu)$ (see, e.g., [Stahl and Totik 92, Appendix A] for relevant definitions).

Thus, heuristically,

$$\log |P_n(z)| \sim n \left(-\log \operatorname{cap}(S(\mu)) + \int d\omega(z) \log(z - x) \right).$$

In words, the exponential growth of $P_n(z)$ for a fixed $z \in \mathbb{C} \setminus [0, 1]$ depends exactly on the quantity $-\log \operatorname{cap}(S(\mu)) + \int d\omega(z) \log(z - x)$.

Now assume that our heuristic formula is valid for $z \in \mathbb{C} \setminus S(\mu)$. (Note that this assumption is not guaranteed by [Stahl and Totik 92, Theorem 3.1.1(ii)].) With this assumption, the logarithmic potential is a
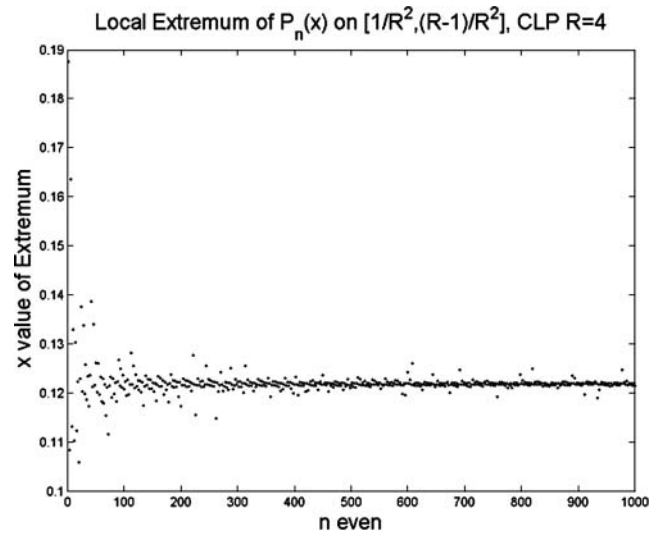

FIGURE 33. x-value of local extremum of $P_n(x)$ on $[1/R^2, (R-1)/R^2] = [1/16, 3/16]$ as a function of n, CLP $R = 4$.
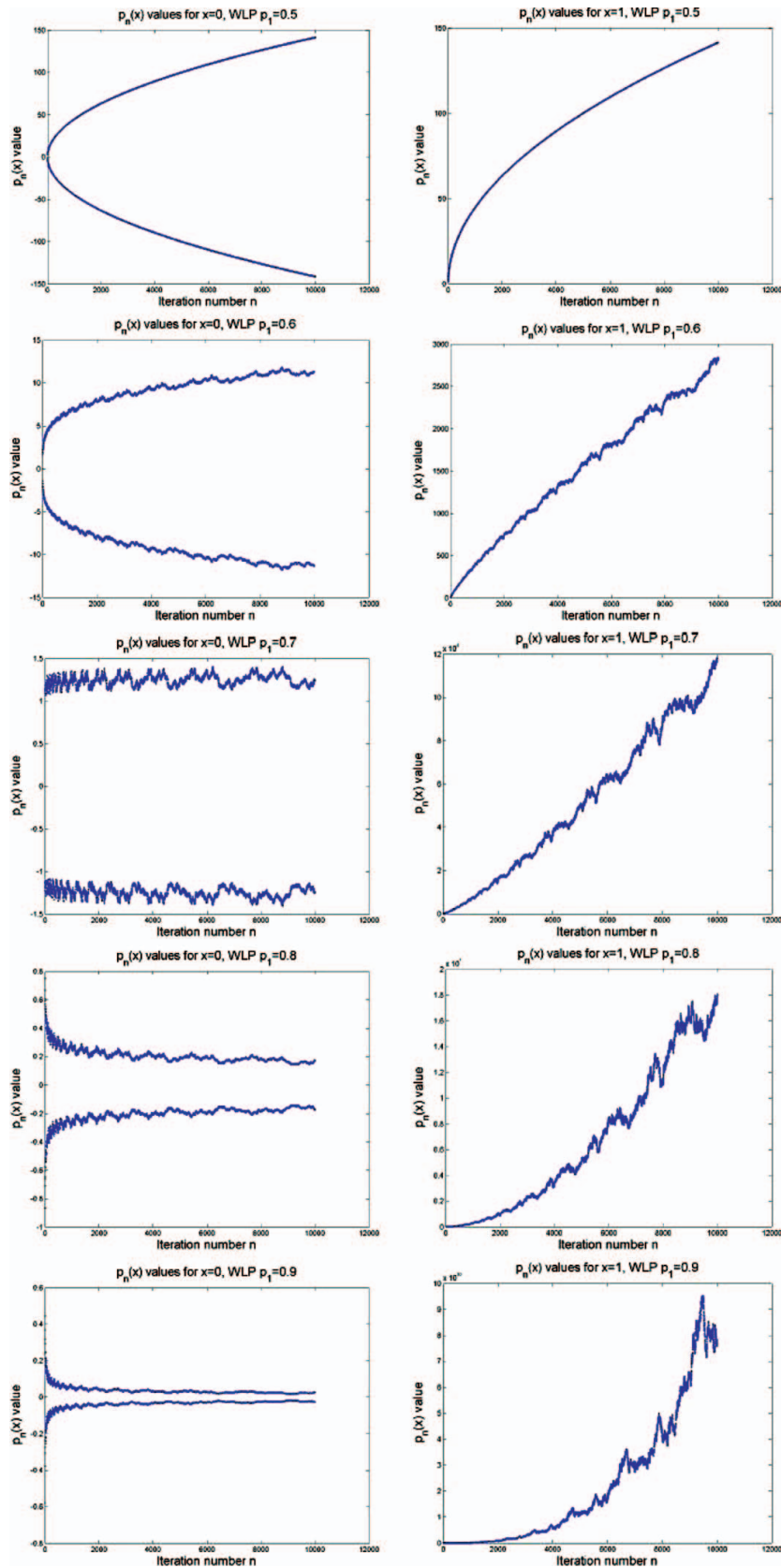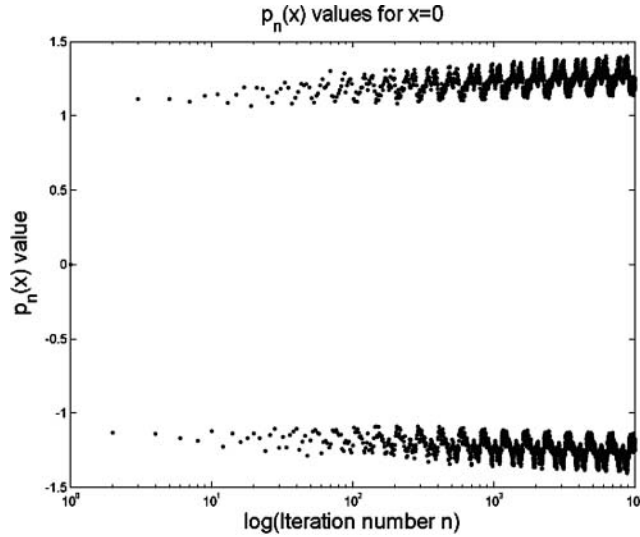
FIGURE 34. $P_n(x)$ values vs. n for $x = 0, 1$ plotted for the WLP $p_1 = 0.5, 0.6, 0.7, 0.8, 0.9$ families (color figure available online).

FIGURE 35. $P_n(0)$ values vs. n logarithmically scaled in the x-axis for WLP $p_1 = 0.7$.

smooth function in the interval $(1/3, 2/3)$, so it can be approximated by its second-order Taylor polynomial at the center point $z = 1/2$. Since this point is a maximum by symmetry, the graph of the Taylor polynomial is a parabola of the desired shape. A similar approximation argument, which can no longer use symmetry, can be made for other intervals in the complement of the Cantor set, $[0, 1] \setminus \text{supp}(\mu)$. This heuristic therefore explains the approximate Gaussian observations of Figures 15, 16, 17, and 29.

7.   WLP AS A FUNCTION OF *n* FOR FIXED *x*

For the classical Legendre polynomials on $[0, 1]$, we find structure in the values of $P_n(x)$ as functions of n for fixed x. As an example, for $x = 0$, $P_n(x) = (-1)^n \sqrt{2n+1}$, and for $x = 1$, $P_n(1) = \sqrt{2n+1}$. The computations of $P_n(0)$ and of $P_n(1)$ are shown at the top of Figure 34. These algebraic relations are a renormalization of the behavior of the classical Legendre polynomials $\widetilde{P}_n$ on $[-1, 1]$, where we recall that $\widetilde{P}_n(1) = 1$, $\widetilde{P}_n(-1) = (-1)^n$, and $||\widetilde{P}_n||^2_{L^2[-1,1]} = 1/(n + 1/2)$ for $n \geq 1$ [Gautschi 04]. We now increase the WLP weight p_1 at the points $x = 0, 1$. As a result, we see a perturbation of the behavior of the classical Legendre polynomials (on $[0, 1]$) in Figure 34.

For $p_1 \approx 0.7$, a transition seems to occur in the behavior of $\{P_n(0)\}^\infty_{n=1}$. At this transition, we appear to have a multiplicative periodic function $P_n(0)$, i.e., a function $f : \mathbb{Z}^+ \to \mathbb{R}$ where for some $a > 0$ we have $f(ax) = f(x)$ for all x. For $p_1 = 0.7$, we can logarithmically scale the x-axis as in Figure 35 to see a nearly multiplicative periodic function. For other p_1, we evidently have a multiplicative

periodic function $P_n(0)/n^\beta$ for an appropriate choice of $\beta = \beta(p_1)$.

For generic[1] $x \in [0, 1]$, if we plot the vectors $(P_n(x), P_{n+1}(x))$ in the WLP $p_1 = 0.5$ (i.e., classical) case, then these vectors are attracted to an ellipse as $n \to \infty$. This ellipse is centered at the origin, and its axes and orientation vary with x. Also, the vectors $(P_n(x), P_{n+1}(x))$ rotate around the ellipse in a periodic way. That is, for a certain $k > 1$ that depends on x (where $k \in \mathbb{Z}$ is the period), $d((P_n(x), P_{n+1}(x)), (P_{n+k}(x), P_{n+k+1}(x))) < \epsilon$ for some small $\epsilon > 0$. Geometrically speaking, $(P_n(x), P_{n+1}(x), n) \in \mathbb{R}^3$ travels along a helix near the surface of an ellipsoidal cylinder. Thus, plotting $(P_n(x), P_{n+1}(x))$ projects this helix onto the plane. In Section 8, we focus on the behavior of $(P_n(x), P_{n+1}(x))$ for generic $x \in [0, 1]$. For now, we merely note the contrast between the images of generic and nongeneric points.

As observed for $x \in \{\{0\}, \{1\}\}$ (a set of two nongeneric points), increasing p_1 perturbs the dynamics of the vectors $(P_n(x), P_{n+1}(x))$. Therefore, increasing p_1 should result in perturbed dynamics for other nongeneric x. To this end, consider $x \in \{\{0.25\}, \{0.5\}, \{0.75\}\}$. For the classical Legendre polynomials on $[0, 1]$, these x-values yield finite attractors for $\{(P_n(x), P_{n+1}(x))\}^\infty_{n=1}$. These attractors have three, four, and six points, respectively. We call the corresponding number of points k_x. The vectors $(P_n(x), P_{n+1}(x))$ travel in a clockwise fashion about the k_x attracting points, as n increases. When we increase p_1, the dynamics of $(P_n(x), P_{n+1}(x))$ for $x \in \{\{0.25\}, \{0.5\}, \{0.75\}\}$ change dramatically, as we see in Figures 36 and 37. Instead of cycling ever closer to k_x attracting points, the vectors $(P_n(x), P_{n+1}(x))$ cycle through k_x fractal spiral arms, as we see in Figure 37.

However, in the case that $p_1 > 0.5$, the attractor of these spiral arms is difficult to determine. By measuring the distance of $(P_n(x), P_{n+1}(x))$ from $(0, 0)$, it seems that the spirals are bounded away from the origin as $n \to \infty$. Therefore, by the symmetry apparent from Figures 36 and 37, $(P_n(x), P_{n+1}(x))$ should be attracted to a (fractal) ellipse, or a finite set of k_x points. As a further contrast to the $p_1 = 0.5$ behavior, we see from Figure 37 that $(P_n(x), P_{n+1}(x), n) \in \mathbb{R}^3$ travels along a "fractal helix" with radius decreasing in n.

---

[1] By a generic point we mean a point chosen, with respect to a uniform distribution, among a suitable set of (rational) values in floating-point arithmetic. In all cases, we treat only x representable in double-precision floating-point arithmetic.
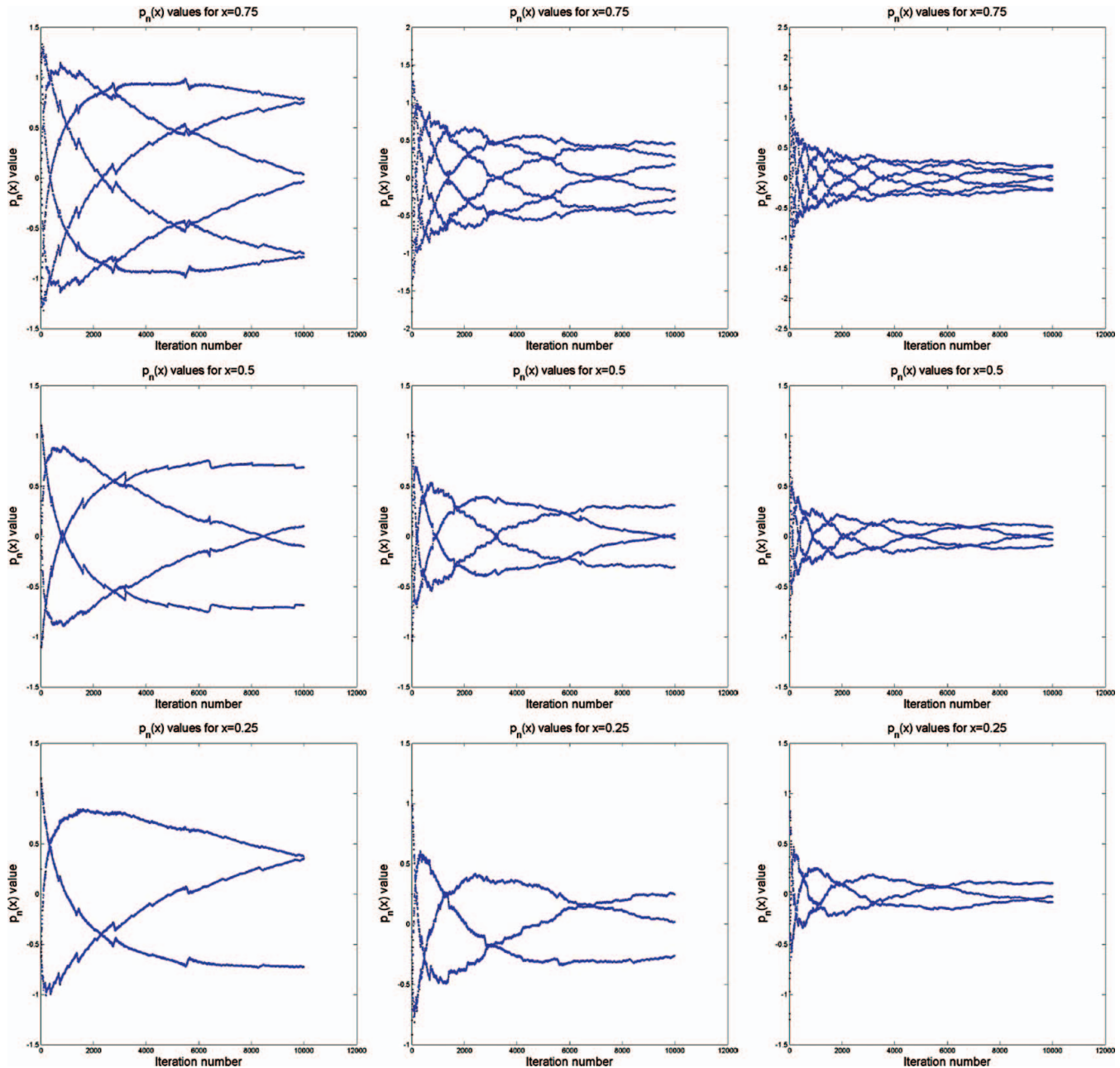
FIGURE 36. $P_n(x)$ values vs. n for $x = 0.75, 0.5, 0.25$ plotted for the WLP $p_1 = 0.6, 0.7, 0.8$ families. Note that for $p_1 = 0.5$, we would get solid horizontal lines (color figure available online).

8. WLP AND CLP DYNAMICS

As promised, we now examine the dynamics of $P_n(x)$ for generic x. Here we examine both WLP and CLP, and we summarize the results in Figure 38. For WLP, we recall for $p_1 = 0.5$ and fixed, generic $x \in [0, 1]$, that there exists an integer $k_x > 1$ such that

$$d((P_n(x), P_{n+1}(x)), (P_{n+k_x}(x), P_{n+k_x+1}(x))) < \epsilon$$
$$(8\text{--}1)$$

for some small $\epsilon > 0$. Here we mean that the sequence of points $\{(P_{n+jk_x}(x), P_{n+jk_x+1}(x))\}_{j=0}^{\infty}$ is periodic of period k_x, up to a small error of ϵ at each step. We therefore make k_x the minimal positive integer satisfying our condition (8–1). If we plot $P_n(x)$ vs. n, we find that $P_n(x)$ is a superposition of k_x sinusoidal functions (see entry $(1, 1)$ in Figure 38). These k_x (approximately) periodic functions are given by $P_{(k_x n+j)}(x)$ for $j \in \{1, 2, \ldots, k_x\}$.

For example, we can see that $k_{0.95} = 14$ by counting the number of distinct periodic functions in the plot of
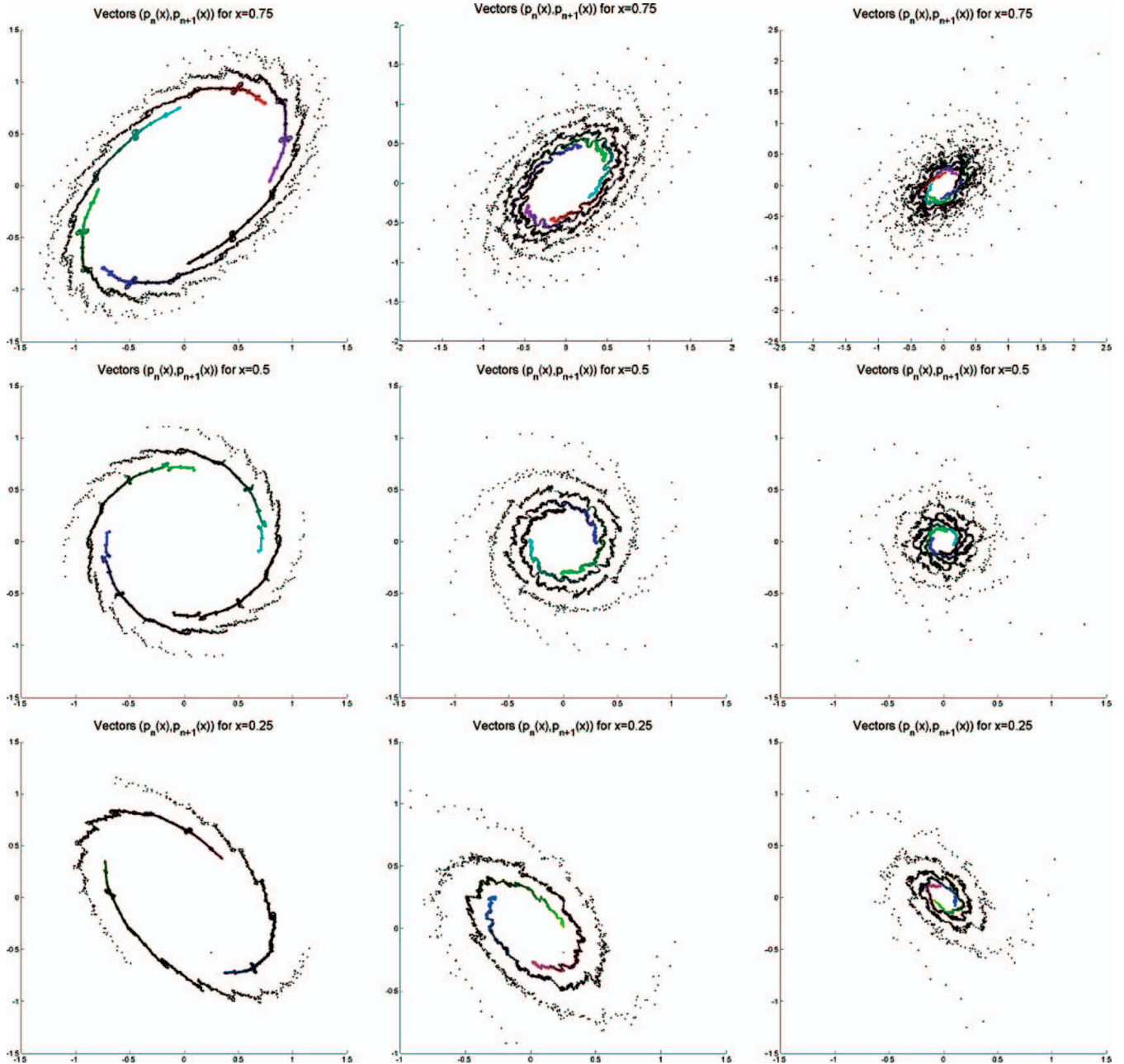
FIGURE 37. Vectors $(P_n(x), P_{n+1}(x))$ for $x = 0.75, 0.5, 0.25$, plotted for the WLP $p_1 = 0.6, 0.7, 0.8$ families (color figure available online).

$P_n(x)$ versus n. Since we essentially have a superposition of phase-shifted cosines, it follows that the distribution of values of $P_n(x)$ is the function $1/\sqrt{1 - y^2}$, suitably rescaled (see entry $(2, 1)$ in Figure 38).

Finally, if we color the iterates $(P_n(x), P_{n+1}(x))$ in a 14-periodic manner, we get entry $(3, 1)$ in Figure 38. In this plot, the point $(P_{n+1}(x), P_{n+2}(x))$ overlaps all points of lower index.

So, what happens when we increase p_1? As in Section 7, we observe a perturbation of the $p_1 = 0.5$ be-

havior. This perturbation becomes more exaggerated the larger p_1 becomes. In the middle column of Figure 38, we show the same plots described in the previous paragraph, for $p_1 = 0.6$. We again choose $x = 0.95$, so $k_{0.95} = 14$, and we observe fourteen vaguely periodic functions. In other words, for $j \in \{1, 2, \ldots, k_x\}$, we see that $P_{(k_x n + j)}(0.95)$ is a perturbed sinusoidal function of n. We can see these perturbations via the distribution function (entry $(2, 2)$) and the plot of $(P_n(x), P_{n+1}(x))$ (entry $(3, 2)$) in Figure 38. That is, the distribution of
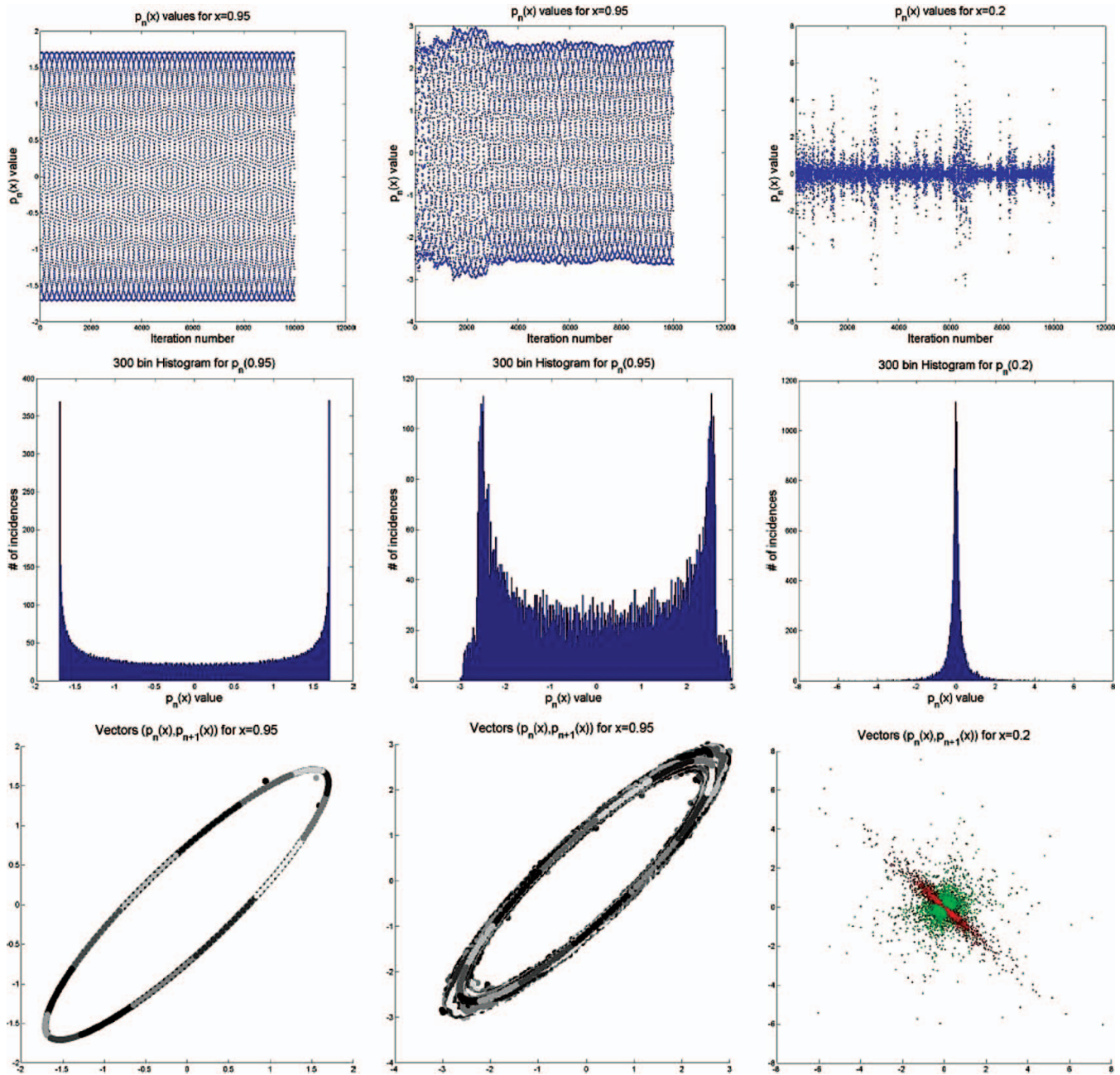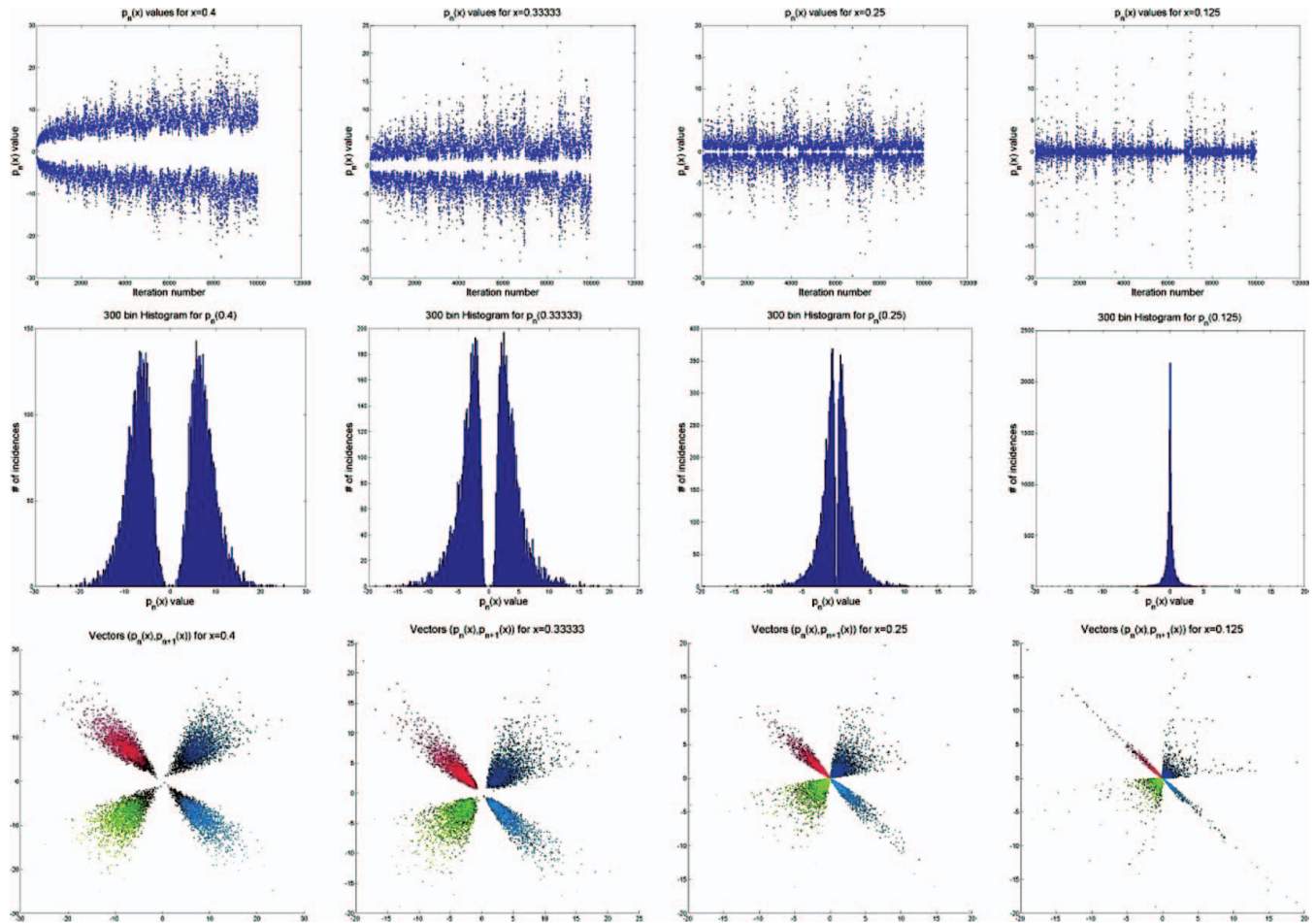
FIGURE 38. Summary of generic point values: p_n values, their histograms, and the vectors $(p_n(x), p_{n+1}(x))$ plotted for the Legendre, WLP $p_1 = 0.6$ and CLP, $R = 4$ polynomial families (color figure available online).

values of $P_n(x)$ is a perturbed version of the function $1/\sqrt{1 - y^2}$, suitably rescaled. Also, the attractor of the vectors $(P_n(x), P_{n+1}(x))$ appears to be a thickened (fractal) ellipse.

The behavior for generic x in the CLP case is displayed in Figure 38 in the rightmost column. As an example, we view the iterates of $x = 1/5 = 1/(R + 1) \in C_R$ for the case $R = 4$. (Recall that $P_n(x)$ grows exponentially for $x \in [0, 1] \setminus C_R$, so we expect more information by viewing

$x \in C_R$.) For generic x, the distribution of $P_n(x)$ values is unclear (Figure 38, entry $(2, 3)$). Nevertheless, the $P_n(x)$ values do seem concentrated around the origin. Also, the vectors $(P_n(x), P_{n+1}(x))$ exhibit a 2-periodic behavior. Specifically, the points $\{(P_{2n}(x), P_{2n+1}(x))\}_{n=1}^{\infty}$ cluster along the line $\{(x, y) \in \mathbb{R}^2 : y = -x\}$ (to abuse notation). Also, the points $\{(P_{2n+1}(x), P_{2n+2}(x))\}_{n=1}^{\infty}$ cluster loosely around the origin. To observe this behavior, note entry $(3, 3)$ in Figure 38.

FIGURE 39. P_n values, their histograms, and the vectors $(P_n(x), P_{n+1}(x))$ plotted for $x = 1/R$, CLP $R = 2.5,\ 3,\ 4$, and 8 polynomial families (color figure available online).

In our investigation, we have found only one non-generic point $x \in C_R \cap [0, 1/2]$ for the CLP case (other than the endpoint $x = 0$). (Note that the symmetry of these $P_n(x)$ across $x = 1/2$ reduces our investigation to $C_R \cap [0, 1/2]$.) Unlike the generic iterates, which demonstrate only 2-periodic behavior, the non-generic point $x = 1/R$ exhibits 4-periodic behavior. The columns of Figure 39 correspond to different p_1 values and the iterates of $x = 1/R$. For $x = 1/R$, the vectors $(P_{4n+j}(x), P_{4n+j+1}(x))$ form four disjoint attractors for $j = \{1, 2, 3, 4\}$. The set $\{(P_{4n+j}(x), P_{4n+j+1}(x))\}_{n=0}^{\infty}$ for $j = 1$ resides in the lower left quadrant; for $j = 2$ this set lives in the upper left quadrant; for $j = 3$ the upper right; and for $j = 4$ the lower right.

9.   CONCLUDING DISCUSSION

Experimental mathematics allows us to see patterns that otherwise would never be observed. At times these patterns allow us to formulate explicit conjectures, and even-

tually proofs may be found to turn conjectures into theorems. But often the story is more complicated. The observed patterns may turn out, on closer inspection, to be only approximately true. No clear-cut conjectures emerge that are truly supported by the experimental evidence. In such cases, what should we do?

We could simply discard the experimental results and move on. But the approximate patterns that we observe may be of great interest. The experiment might be trying to tell us something that we are not quite able to capture in the conventional format of mathematical statements. Experimental science is often messy in exactly this way, and we think it would be a shame to limit experimental mathematics to only the clean paradigm.

We see the results reported in this paper in exactly this light. We do have clean-cut conjectures on the r_n values in Section 2 and boundedness for WLP in Section 3, but beyond that we only have messy evidence. We see some CLP Dirichlet kernels that look more like approximate identities than most Dirichlet kernels. We

are able to relate this to the small size of the r_n coefficients. The experimental evidence suggests that we will not find a sequence with r_n converging to zero. So we cannot offer a conjecture analogous to the results of [Strichartz 06] about uniform convergence of certain special partial sums of the orthogonal polynomial expansion of an arbitrary continuous function. However, the results of [Strichartz 06] suggest that perhaps such a statement might hold only for special values of R, and we have examined only a few choices of R.

The approximate equalities for CLP discussed in Section 5 appear very striking when one looks at the graphs of the polynomials. It is on closer inspection that one observes the deviation from equality. A clean conjecture might say that the deviation goes to zero in some limit, but the evidence does not really support such a conjecture. Nevertheless, we find the approximate equalities intrinsically interesting.

Similarly, a glance at the graphs of CLP on the gaps suggests they are close to being Gaussian. Of course one comes to expect Gaussian limits in many mathematical situations. But here in Section 6, on closer inspection, we see a decided deviation from the Gaussian model. In this case we believe there is a true limit law; we just have not been able to find it.

Perhaps the most interesting contribution of this paper is the dynamical perspective discussed in Sections 7 and 8. Here we may be excused from offering explicit conjectures on the grounds that the pictures offer a view of significant structures that were previously unrecognized. We hope that others will be inspired to investigate the dynamics perspective in a systematic way.

ACKNOWLEDGMENTS

REFERENCES

[Barnsley et al. 83a] M. F. Barnsley, J. S. Geronimo, and A. N. Harrington. "Infinite-Dimensional Jacobi Matrices Associated with Julia Sets." *Proc. Amer. Math. Soc.* 88:4 (1983), 625–630.

[Barnsley et al. 83b] M. F. Barnsley, J. S. Geronimo, and A. N. Harrington. "On the Invariant Sets of a Family of Quadratic Maps." *Comm. Math. Phys.* 88:4 (1983), 479–501.

[Barnsley et al. 85] M. F. Barnsley, J. S. Geronimo, and A. N. Harrington. "Almost Periodic Jacobi Matrices Associated with Julia Sets for Polynomials." *Comm. Math. Phys.* 99:3 (1985), 303–317.

[Bessis and Moussa 83] D. Bessis and P. Moussa. "Orthogonality Properties of Iterated Polynomial Mappings." *Comm. Math. Phys.* 88:4 (1983), 503–529.

[Bird et al. 06] E. J. Bird, S.-M. Ngai, and A. Teplyaev. "Fractal Laplacians on the Unit Interval." *Ann. Sci. Math. Québec* 27:2 (2003), 135–168.

[Coletta et al. 04] K. Coletta, K. Dias, and R. S. Strichartz. "Numerical Analysis on the Sierpinski Gasket, with Applications to Schrödinger Equations, Wave Equation, and Gibbs' Phenomenon." *Fractals* 12:4 (2004), 413–449.

[Dutkay and Jorgensen 06] D. E. Dutkay and P. E. T. Jorgensen. "Iterated Function Systems, Ruelle Operators, and Invariant Projective Measures." *Math. Comp.* 75:256 (2006), 1931–1970 (electronic).

[Fischer 95] H.-J. Fischer. "Recurrence Coefficients of Orthogonal Polynomials with Respect to Some Self-Similar Singular Distributions." *Z. Anal. Anwendungen* 14:1 (1995), 141–155.

[Gautschi 04] W. Gautschi. *Orthogonal Polynomials: Computation and Approximation*, Numerical Mathematics and Scientific Computation. New York: Oxford University Press, 2004.

[Huang and Strichartz 01] N. N. Huang and R. S. Strichartz. "Sampling Theory for Functions with Fractal Spectrum." *Experiment. Math.* 10:4 (2001), 619–638.

[Jorgensen and Pedersen 00] P. E. T. Jorgensen and S. Pedersen. "Dense Analytic Subspaces in Fractal L^2-Spaces." *J. Anal. Math.* 75 (1998), 185–228.

[Kigami 01] J. Kigami. *Analysis on Fractals*, Cambridge Tracts in Mathematics 143. Cambridge, UK: Cambridge University Press, 2001.

[Lund et al. 98] J.-P. Lund, R. S. Strichartz, and J. P. Vinson. "Cauchy Transforms of Self-Similar Measures." *Experiment. Math.* 7:3 (1998), 177–190.

[Laba and Wang 02] I. Laba and Y. Wang. "On Spectral Cantor Measures." *J. Funct. Anal.* 193:2 (2002), 409–420.

[Lau and Wang 93] K.-S. Lau and J. Wang. "Mean Quadratic Variations and Fourier Asymptotics of Self-Similar Measures." *Monatsh. Math.* 115:1–2 (1993), 99–132.

[Mantica 96] G. Mantica. "A Stable Stieltjes Technique for Computing Orthogonal Polynomials and Jacobi Matrices

Associated with a Class of Singular Measures." *Constr. Approx.* 12:4 (1996), 509–530.

[Mantica 97a] G. Mantica. "Quantum Intermittency in Almost-Periodic Lattice Systems Derived from Their Spectral Properties." *Physica D* 103 (1997), 576–589.

[Mantica 97b] G. Mantica. "Wave Propagation in Almost-Periodic Structures." *Physica D* 109 (1997), 113–127.

[Mantica 98a] G. Mantica. "Quantum Intermittency: Old or New Phenomenon?" *J. Phys. IV France* 8 (1998), 253.

[Mantica 98b] G. Mantica. "Fourier Transforms of Orthogonal Polynomials of Singular Continuous Spectral Measures." In *Applications and Computation of Orthogonal Polynomials (Oberwolfach, 1998)*, Internat. Ser. Numer. Math. 131, pp. 153–163. Basel: Birkhäuser, 1999.

[Mantica 00] G. Mantica. "On Computing Jacobi Matrices Associated with Recurrent and Möbius Iterated Function Systems." In *Proceedings of the 8th International Congress on Computational and Applied Mathematics, ICCAM-98 (Leuven). J. Comput. Appl. Math.* 115:1–2 (2000), 419–431.

[Máté et al. 91] A. Máté, P. Nevai, and W. Van Assche. "The Supports of Measures Associated with Orthogonal Polynomials and the Spectra of the Related Selfadjoint Operators." In *Proceedings of the U.S.–Western Europe Regional Conference on Padé Approximants and Related Topics (Boulder, CO, 1988). Rocky Mountain J. Math.* 21:1 (1991), 501–527.

[Oberlin et al. 03] R. Oberlin, B. Street and R. S. Strichartz. "Sampling on the Sierpinski Gasket." *Experiment. Math.* 12:4 (2003), 403–418.

[Owrutsky 05] P. Owrutsky. "Orthogonal Polynomials on Singular Measures" (electronic). Available online (http://www.math.cornell.edu/~orthopoly/).

[Stahl and Totik 92] H. Stahl and V. Totik. "General Orthogonal Polynomials." In *Encyclopedia of Mathematics and Its Applications*, 43. Cambridge, UK: Cambridge University Press, 1992.

[Strichartz 90] R. S. Strichartz. "Self-Similar Measures and Their Fourier Transforms. I." *Indiana Univ. Math. J.* 39:3 (1990), 797–817.

[Strichartz 93a] R. S. Strichartz. "Self-Similar Measures and Their Fourier Transforms. II." *Trans. Amer. Math. Soc.* 336:1 (1993), 335–361.

[Strichartz 93b] R. S. Strichartz. "Self-Similar Measures and Their Fourier Transforms. III." *Indiana Univ. Math. J.* 42:2 (1993), 367–411.

[Strichartz 94] R. S. Strichartz. "Self-Similarity in Harmonic Analysis." *J. Fourier Anal. Appl.* 1:1 (1994), 1 –37.

[Strichartz 98] R. S. Strichartz, "Remarks on: 'Dense Analytic Subspaces in Fractal L^2-Spaces,' by P. E. T. Jorgensen and S. Pedersen. *J. Anal. Math.* 75 (1998), 185–228." *J. Anal. Math.* 75 (1998), 229–231.

[Strichartz 00] R. S. Strichartz. "Mock Fourier Series and Transforms Associated with Certain Cantor Measures." *J. Anal. Math.* 81 (2000), 209–238.

[Strichartz 05] R. S. Strichartz. "Laplacians on Fractals with Spectral Gaps Have Nicer Fourier Series." *Math. Res. Lett.* 12:2–3 (2005), 269–274.

[Strichartz 06] R. S. Strichartz. "Convergence of Mock Fourier Series." *J. Anal. Math.* 99 (2006), 333–353.

[Strichartz and Wong 04] R. S. Strichartz and C. Wong, "The p-Laplacian on the Sierpinski gasket." Nonlinearity 17 (2004), no. 2, 595–616.

[Szegő 75] Gábor Szegő. *Orthogonal Polynomials*, fourth edition, American Mathematical Society, Colloquium Publications, XXIII. Providence: American Mathematical Society, 1975.

[Talagrand 89] M. Talagrand. "A Conjecture on Convolution Operators, and a Non-Dunford–Pettis Operator on L^1." *Israel J. Math.* 68:1 (1989), 82–88.

Steven M. Heilman, Courant Institute of Mathematical Sciences, New York University, New York, NY 10012-1185 (heilman@cims.nyu.edu)

Philip Owrutsky, Division of Engineering and Applied Sciences, Harvard University, Cambridge, MA 02138 (owrutsky@fas.harvard.edu)

Robert S. Strichartz, Department of Mathematics, Cornell University, Ithaca, NY 14850-4201 (str@math.cornell.edu)